JPL PUBLICATION 85-64

Fundamental Study of Flow Field Generated by Rotorcraft Blades Using Wide-Field Shadowgraph

S. P. Parthasarathy
Y. I. Cho
L. H. Back

October 1, 1985

NASA
National Aeronautics and
Space Administration

Jet Propulsion Laboratory
California Institute of Technology
Pasadena, California

TECHNICAL REPORT STANDARD TITLE PAGE

1. Report No. JPL PUB 85-64	2. Government Accession No.	3. Recipient's Catalog No.
4. Title and Subtitle Fundamental Study of Flow Field Generated by Rotorcraft Blades Using Wide-Field Shadowgraph		5. Report Date October 1, 1985 6. Performing Organization Code
7. Author(s) S.P. Parthasarathy, Y.I. Cho, L.H. Back		8. Performing Organization Report No.
9. Performing Organization Name and Address JET PROPULSION LABORATORY California Institute of Technology 4800 Oak Grove Drive Pasadena, California 91109		10. Work Unit No. 11. Contract or Grant No. NAS7-918 13. Type of Report and Period Covered JPL Publication
12. Sponsoring Agency Name and Address NATIONAL AERONAUTICS AND SPACE ADMINISTRATION Washington, D.C. 20546		14. Sponsoring Agency Code CY-505-42-11-04-55
15. Supplementary Notes		

16. Abstract

The vortex trajectory and vortex wake generated by helicopter rotors were visualized using a wide-field shadowgraph technique. Use of a retro-reflective Scotchlite screen made it possible to investigate the flow field generated by full-scale rotors. Tip vortex trajectories were visible in shadowgraphs for a range of tip Mach number of 0.38-0.60. The effect of the angle of attack was substantial. At an angle of attack greater than 8 degrees, the visibility of the vortex core was significant even at relatively low tip Mach numbers. The theoretical analysis of the sensitivity was carried out for a rotating blade. This analysis demonstrated that the sensitivity decreases with increasing dimensionless core radius and increases with increasing tip Mach number. The threshold value of the sensitivity was found to be 0.0015, below which the vortex core is not visible and above which it is visible. The effect of the optical path length was also discussed. Based on this investigation, it is concluded that the application of this wide-field shadowgraph technique to a large wind tunnel test should be feasible. In addition, two simultaneous shadowgraph views would allow three-dimensional reconstruction of vortex trajectories.

17. Key Words (Selected by Author(s))	18. Distribution Statement
Aeronautics (General) Research and Support Facilities (Air) Instrumentation and Photography	unclassified, distribution unlimited

19. Security Classif. (of this report)	20. Security Classif. (of this page)	21. No. of Pages	22. Price
unclassified	unclassified		

JPL PUBLICATION 85-64

Fundamental Study of Flow Field Generated by Rotorcraft Blades Using Wide-Field Shadowgraph

S. P. Parthasarathy
Y. I. Cho
L. H. Back

October 1, 1985

NASA
National Aeronautics and
Space Administration

Jet Propulsion Laboratory
California Institute of Technology
Pasadena, California

The research described in this publication was carried out by the Jet Propulsion Laboratory, California Institute of Technology, under a contract with the National Aeronautics and Space Administration.

TABLE OF CONTENTS

Abstract

The vortex trajectory and vortex wake generated by helicopter rotors were visualized using a wide-field shadowgraph technique. Use of a retro-reflective Scotchlite screen made it possible to investigate the flow field generated by full-scale rotors. Tip vortex trajectories were visible in shadowgraphs for a range of tip Mach number of 0.38 ~ 0.60. The effect of the angle of attack was substantial. At an angle of attack greater than 8 degrees, the visibility of the vortex core was significant even at relatively low tip Mach numbers. The theoretical analysis of the sensitivity was carried out for a rotating blade. This analysis demonstrated that the sensitivity decreases with increasing dimensionless core radius and increases with increasing tip Mach number. The threshold value of the sensitivity was found to be 0.0015, below which the vortex core is not visible and above which it is visible. The effect of the optical path length was also discussed. Based on this investigation, it is concluded that the application of this wide-field shadowgraph technique to a large wind tunnel test should be feasible. In addition, two simultaneous shadowgraph views would allow three-dimensional reconstruction of vortex trajectories.

LIST OF FIGURES

1. INTRODUCTION

The objective of the task was to visualize the helicopter rotor wake to determine the geometry and structure of the tip vortices using the wide-field shadowgraphy technique. The vortices should be observed for several blade passages above the rotor which is thrusting downward in the present case. An important condition in the design of the experiment was to conduct the experiment at nearly full scale (i.e., the distance between the screen and rotor blade should be in the order of 3-9 m) so that the system of measurement could apply to an actual wind tunnel test. Experiments were conducted on a tail rotor, which is considerably smaller than the main rotor, but the distances from light source to screen were kept large enough to be approximately full scale. The largest distance between the axis of the rotor and the screen was 6.4 m.

It was expected that useful shadows would result from the natural density changes in the vortex cores associated with low pressures. The sensitivity of the shadowgraphs which depends on the second derivative of the density field was not known. It was, therefore, necessary to determine the visibility experimentally.

Addition of a fluid with different density was also investigated to determine the characteristics of the resulting shadowgraphs. This was done by using a hot air gun during some of the tests.

2. BACKGROUND OF FLOW VISUALIZATION TECHNIQUES

2.1 Schlieren Technique

Fluid flows are visualized by many optical techniques, as is well known. Of these, Schlieren photography is practically restricted to a field of view of about 50 cm because of the necessity of using high quality mirrors in the technique. Interferometry which senses the density field is very delicate and has the same field of view limitation.

Schlieren photography has been used to visualize the tip vortex flow by Tangler[1] using a small scale setup. The rotors were about 1 ft radius. The wake of each blade can be seen for approximately one revolution of the blade before it vanishes by diffusive interaction. Kokurek and Tangler[2] developed an improved wake representation from small scale Schlieren studies.

Moire Schlieren can be used for large field flow visualization but the method is more complicated than simple shadowgraphy.

2.2 Shadowgraphy Technique

Shadowgraphy is the simplest optical technique. Here, second derivatives of density are sensed as light variations on the screen. When a point source illuminates a large screen, density changes in the test section between the light source and the screen cause shadows to be cast on the screen. This shadow can be seen directly or can be photographed by a camera provided there is enough light to produce a good exposure. Usually, light is insufficient for a good exposure if the screens are ordinary, white surfaces.

However, when the screens are treated with retroreflecting Scotchlite (a 3M product), the light gathered by a camera placed as close as possible to the point source of light is sufficient for a good exposure. A stroboscope is generally used to freeze the motion during the time the camera shutter is open.

Shadowgraphy reveals naturally occurring density changes in the flow as well as those changes induced by deliberate introduction of tracers of different densities such as hot air, carbon dioxide gas, etc. In the present application, tip vortices from rotors cause enough density changes to be visible without the introduction of tracers. However, tracers can be used to examine the flow field in regions where there are no naturally occurring density changes.

2.3 Use of Smoke

In addition to the optical technique, introduction of dense smoke into the flow field is a method that has been used to examine the position of tip vortices and the location of vortex sheets which reveal their presence by the discontinuity in smoke streaks. Many photographs using this method are given in the report by Landgrebe[3].

The location of the inboard vortex sheet is shown as discontinuities in the smoke streaks and the tip vortices are seen by smoke surrounding the cores which are clear of smoke. The location of cores is made visible only in those places where the smoke gets in and this region is probably at a fixed azimuthal coordinate. If there is a circumferential velocity in the rotor wake, the smoke would tag successive vortex cores at different azimuthal coordinates and lead to a misleading interpretation of the flow field with regard to the position of vortex cores. Accurate sheet lighting of a narrow region at a fixed azimuth would overcome this problem, however. This may not be easy to do in practice.

Shadowgraphy reveals the shadow all along the vortex core because there is no need for a tracer. If two views of the same field are taken simultaneously, it should be possible to obtain accurately the coordinates of the spiralling tip vortex as a function of time with no assumptions on the nature of the flow field and with no disturbance to the flow.

3. EXPERIMENTAL FACILITY

3.1 Rotor Blade Assembly

To simulate flow fields generated by rotorcraft blades, a tail rotor together with the gear box (Hughes Model 300) was obtained through the Sheriff's Department, County of Los Angeles. The symmetric blade was rectangular with chord length of 0.12 m (NACA airfoil 0015) . The distance from the center of rotation to the blade tip was 0.65 m. The designed-operating speed of this rotor was 2900-3100 rpm with a torque of 269 N-m. At 3100 rpm, the blade tip speed was found to be 210 m/s (i.e., Mach number 0.61) and the required electric motor power was 18.6 Hp. The schematic

diagram of the rotor blade assembly is shown in Fig. 1, including the tail rotor (2-blades), gear box, pitch angle controller, variable pulley and sheaves, 20 Hp motor (440V, 25 Amp), adjustable motor base, and reduced voltage starter. A picture of the system is also shown in Fig. 2.

The rotor test assembly was balanced with the Vibrex Track and Balance System made by the Chadwick and Helmuth Company (El Monte, CA). During the balancing test, the maximum operational speed of 3100 rpm was obtained.

3.2 Limitation of the Rotor Blade Assembly

As mentioned earlier, the designed-operating speed of the tail rotor (Hughes Model 300) was 3100 rpm (i.e., Mach number ≈ 0.61). However, to obtain a Mach number of 0.7, the rotor would have to rotate at 3560 rpm, which may be beyond the design limit of this rotor. In addition, tail rotor blades were retired after 3000 flight hours logged by the L. A. County Sheriff's Department. Therefore, from a safety point of view, it was advisable to stay within the designed maximum limit (i.e., 3100 rpm). This limited obtaining a higher Mach number than 0.61 from the rotor blade assembly.

The limitation of keeping the tip Mach number below 0.61 would not be serious if shadowgraphic observations of the tip vortices were possible at the lower Mach numbers. This proved to be the case.

3.3 The Shadowgraph Setup

The setup with camera focused on the shadow on the Scotchlite screen is shown in Fig. 3. Stroboscopic observations were made by driving the strobe lamp from the signal from the photoprobe, thus automatically freezing the rotor blade motion at a fixed location throughout the test. In addition, the use of slip/sinc control in the Strobex System (made by the Chadwick and Helmuth Company) allowed us to observe shadowgraphs from slowly moving rotor blades. The magnetic pickup mounted near the shaft connecting the rotor clutch device to the electric motor measured the shaft rpm which was 2/3 of the rotation speed of the rotor because of the gear ratio used in the device. Scotchlite shadowgraphs were observed at two distances, viz 6.4 m between the rotor and screen and also 4.4 m. The corresponding distances between the light source and screen were 11 m and 7.8 m, respectively. These distances could be expected in applications of this technique when the strobe source is located in a large wind tunnel.

4. EXPERIMENTAL RESULTS AND DISCUSSION

Many Shadowgraphs taken at different rpm and angles of attack are enclosed in the report (Figs. 4-16). The values of the relevant parameters are given in the figure captions. The vortices and the flow field near them, made visible by the use of hot air injection, can be seen and interpreted readily. Note that since the blades are at different rotational locations in the figures, the vortex system extends beyond the instantaneous projections of the blades.

4.1. Visibility

Figure 4 shows the shadowgraph of the rotor at ℓ = 4.4 m at 3200 rpm (i.e., M_T= 0.64) and at 12° angle of attack. The vortex cores are seen as two thin spirals emanating from the two blade tips. On the right, hot air from a hair dryer circulates around the tip vortex and shows the circulating flow. On the left, only the density gradient occurring naturally in the core makes the vortex visible. At the extreme right and left edges, the shadows are denser because the light rays pass tangentially through the vortices. Three dark spots are visible on the left vertically showing these edges. The vortices are distorted at this condition of high angle of attack and high rpm. Figure 5 shows another phase of the rotor at the same conditions. Distortions are clearly visible on the left. It is worth noting that these shadowgraph pictures give detailed information on the entire vortex trajectory, the vortex core size and the wake around the vortex core, which can provide useful input for the computer modeling of the helicopter rotor performance[3].

Photographs taken from a larger optical path length ℓ = 6.4 m are considered next. In Fig. 6 at 1920 rpm (i.e., M_T= 0.38) and α = 4°, the tip vortex at the right is just visible (or very faint) above the hot air gun. There was no hot air flow from the gun except for a slight convection current from a previous hot run. In Fig. 7, at the same flow conditions as in Fig. 6, the flow near the tip when the hot air flow is on, together with the faint vortex (spot) are seen. In Figs. 8 and 9, the angle of attack is still 4° but the speed is higher viz 2763 rpm (i.e., M_T= 0.55). Spiralling vortices are slightly visible and one dark spot is clearly seen just above the heat gun. Therefore, the threshold value of the sensitivity was determined from the test with α = 4° and M_T = 0.38, which yielded a just visible tip vortex core as shown in Figs. 6 and 7. Of note is that the sensitivity analysis (see Appendix) resulted in the threshold value of S = 0.00025.

At a higher angle of attack α = 8°, the spirals are clearer as seen in Fig. 10 with hot air injection at the right. Figs. 11 and 12 at α = 8°, 2890 rpm (i.e., M_T= 0.58) show the vortices clearly. Distortions in the spirals are also seen. Figs. 13 to 16 are for α = 14°. The visibility of these vortices is similar to those at 8°. Of note is that the values of the sensitivity corresponding to the angle of attack α = 8, 12 and 14° were obviously above the threshold value of S = 0.00025. These details are given in the Appendix.

As mentioned earlier, two different beam lengths ℓ (i.e., distance between the rotor and screen) were used. In Figs. 4 and 5, the beam length ℓ was 4.4 m and in Figs. 6 to 16, it was 6.4 m. Although the theory shows that the sensitivity is linearly proportional to the beam length, the contribution of the beam length was not significant in these shadowgraph pictures when ℓ was changed from 4.4 to 6.4 m.

Other photographs not included in this report show similar characteristics. The table shows the experimental conditions with brief comments on the results.

4.2 Experimental Determination of Vortex Core Radius r_o

The size of the vortex core was experimentally determined from the shadowgraph picture given in Fig. 5 (i.e., $\alpha = 12°$ and $M_T = 0.64$). Since the rotor radius is 0.65 m, one can calculate the scale-up factor between the real size and shadowgraph image. This results in a value of the vortex core radius of 7.6 mm for the case shown in Fig. 5. Thus, the ratio of the vortex core radius to the chord r_o/c is 0.063.

4.3 Experimental Determination of the Axial Velocity in the Wake

Most shadowgraph pictures in Figs. 5 and 6, 10-16 show, typically, three vortex cores (for example, see three dark spots at the left side in Fig. 4). Thus, by knowing the rpm and the distance between two vortex cores, one can calculate the axial velocity due to the hovering motion of rotors. For the case of 3200 rpm and an angle of attack of 12° in Fig. 4, the axial velocity was calculated to be 20.4 m/s.

Further discussion of experimental data and analysis is given in the Appendix.

5. CONCLUSIONS AND RECOMMENDATIONS

Tip vortex trajectories were visible in shadowgraphs for a range of tip Mach numbers from 0.38 to 0.6. The angles of attack ranged from 4° to 14°. Visibility improves with speed and angle of attack. The effect of the angle of attack α was substantial. At an angle of attack greater than 8 degrees, the visibility is significant even at relatively low tip Mach numbers. It can be expected that at higher tip speeds, visibility would be even better. In addition, the size of the vortex core and the axial velocity during the hovering motion could be determined experimentally.

It is therefore concluded that the application of the technique to a large wind tunnel would be successful. Simultaneous, multiple views would be the next step to get three dimensional information on the tip vortices, the vortex core radius and the axial velocity.

ACKNOWLEDGMENT

Mr. John Kendall from the County of Los Angeles, Sheriff's Department provided the rotor and its clutch box, and Mr. J. Chadwick from the Chadwick-Helmuth Company balanced the rotor with his Vibrex Track and Balance System.

The authors also express appreciation to Messrs. J. Godley, B. Green and R. Smither for their contributions in fabrication and assembly of the test facility and to Dr. Ken Harstad for his assistance in the calculation of the sensitivity function.

REFERENCES

1. Tangler, J. L., "The Design and Testing of a Tip to Reduce Blade Slap," 31st Annual Meeting of the American Helicopter Society, May 1975, preprint no. 963.

2. Kokurek, J. D., and Tangler, J. L., "A Prescribed Wake Lifting Surface Hover Performance Analysis," Journal of the American Helicopter Society, Vol. 22, pp. 24-35, 1977.

3. Landgrebe, A. J., "An Analytical and Experimental Investigation of Helicopter Rotor Hover Performance and Wake Geometry Characteristics," USAAMRDL Technical Report 71-24, June 1971.

TABLE

No	α	M_T	rpm	Heat	Visibility of Vortex	Comments
17	4	0.38	1920	No	Yes	Faintly
17	"	"	"	Yes	Yes	Vortex is faint
17	"	"	"	Yes	No	
17	"	0.48	2454	No	Yes	
17	"	"	"	No	Yes	Faint
17	"	"	"	Yes	No	Entrance flow is visible
17	"	"	"	Yes	No	
17	"	0.54	2763	No	Yes	Two loops
17	"	"	"	No	Yes	Two loops
17	"	"	"	Yes	Yes	One loop
13-2	8	0.38	1910	Yes	Yes	1 loop and 3 spiral heat flows
13-2	"	"	"	Yes	Yes	1 sharp loop & heat flow
13-3	"	"	"	Yes	Yes	2 loops & heat flow
13-4	"	"	"	Yes	Yes	2 loops & heat
14-5	"	0.48	2460	Yes	Yes	2 Cores & hot flow
14-6	"	"	"	Yes	Yes	Distorted helices
14-7	"	"	"	Yes	Yes	2 helices
14-8	"	"	"	Yes	Yes	2 helices
15-9	"	0.54	2750	Yes	Yes	2 distorted helices
15-10	"	"	"	Yes	Yes	2 distorted helices
15-11	"	"	"	Yes	Yes	2 sharp distorted helices + flow
15-12	"	"	"	Yes	Yes	Distorted
16-1	"	0.57	2890	No	Yes	2 distorted helices
16-2	8	"	"	No	Yes	2 distorted helices
16-3	"	"	"	No	Yes	2 distorted helices
16-4	"	"	"	No	Yes	2 distorted helices
16-5	"	"	"	No	Yes	2 distorted helices
16-6	"	"	"	No	Yes	2 distorted helices
16-7	"	"	"	No	Yes	Very distorted
16-8	"	"	"	No	Yes	2, vortex shows jilter in 5 exposures
16-9	"	"	"	No	Yes	2 distorted helices
16-10	"	"	"	Yes	Yes	2 distorted helices + heat
16-11	"	"	"	Yes	Yes	2 distorted helices + heat
16-12	"	"	"	Yes	Yes	2 distorted helices + heat
18-1	14	0.38	1908	No	Yes	2 distorted helices
18-2	"	"	"	No	Yes	2 distorted helices
18-3	"	"	"	Yes	Yes	2 helices + heated flow
18-4	"	"	"	Yes	Yes	2 helices + heated flow
18-5	"	0.48	2454	No	Yes	2 distorted helices
18-6	"	"	"	No	Yes	2 distorted helices
18-7	"	"	"	Yes	Yes	2 distorted helices + hot flow
18-8	"	"	"	Yes	Yes	2 distorted helices + hot flow
18-9	"	0.54	2762	No	Yes	2 helices
18-10	"	"	"	No	Yes	2 helices
18-11	"	"	"	Yes	Yes	2 distorted helices + flow
18-12	"	"	"	Yes	Yes	2 distorted helices + flow

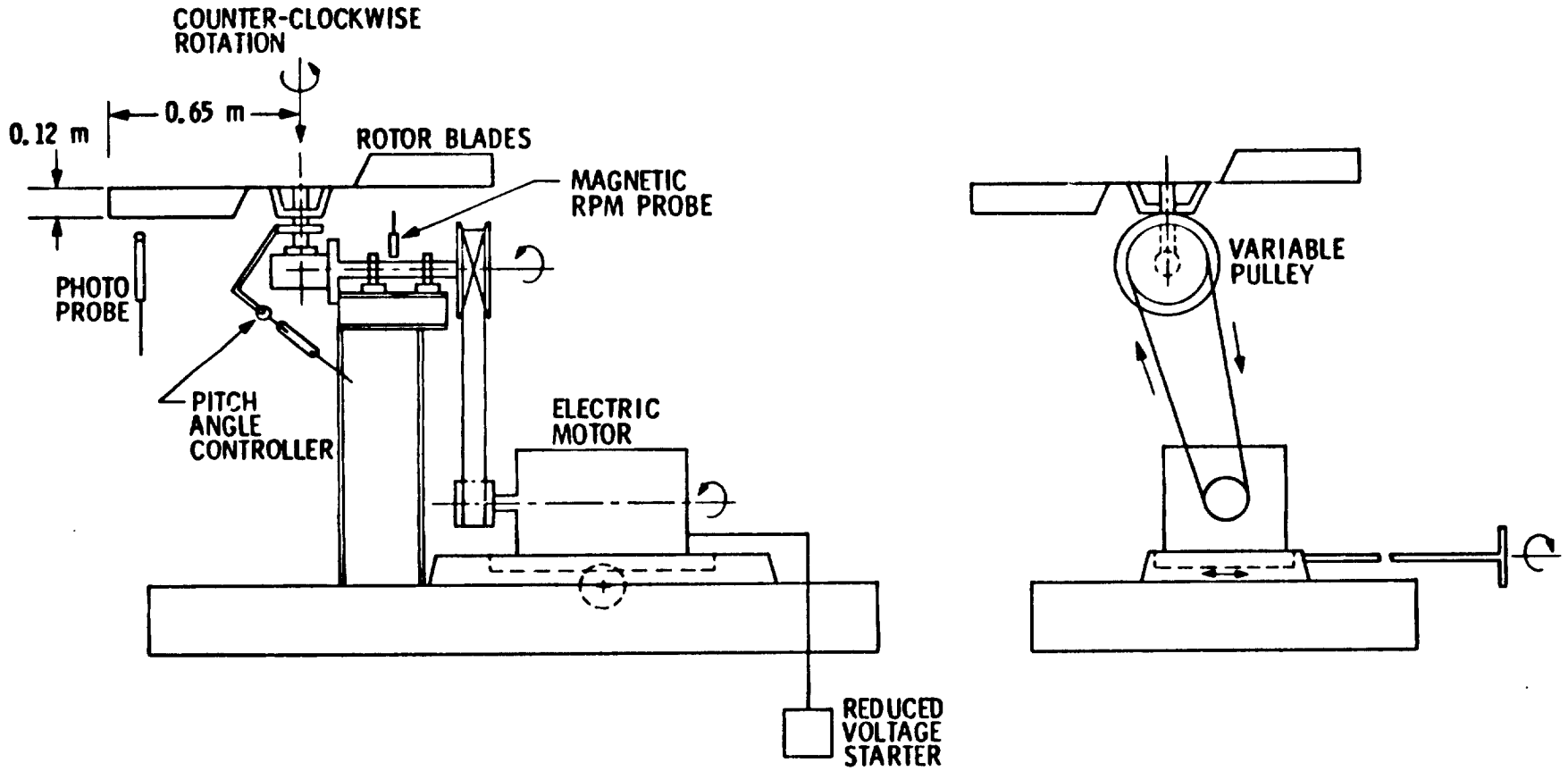

Fig. 1 Schematic diagram of Rotorblade Experimental Setup.

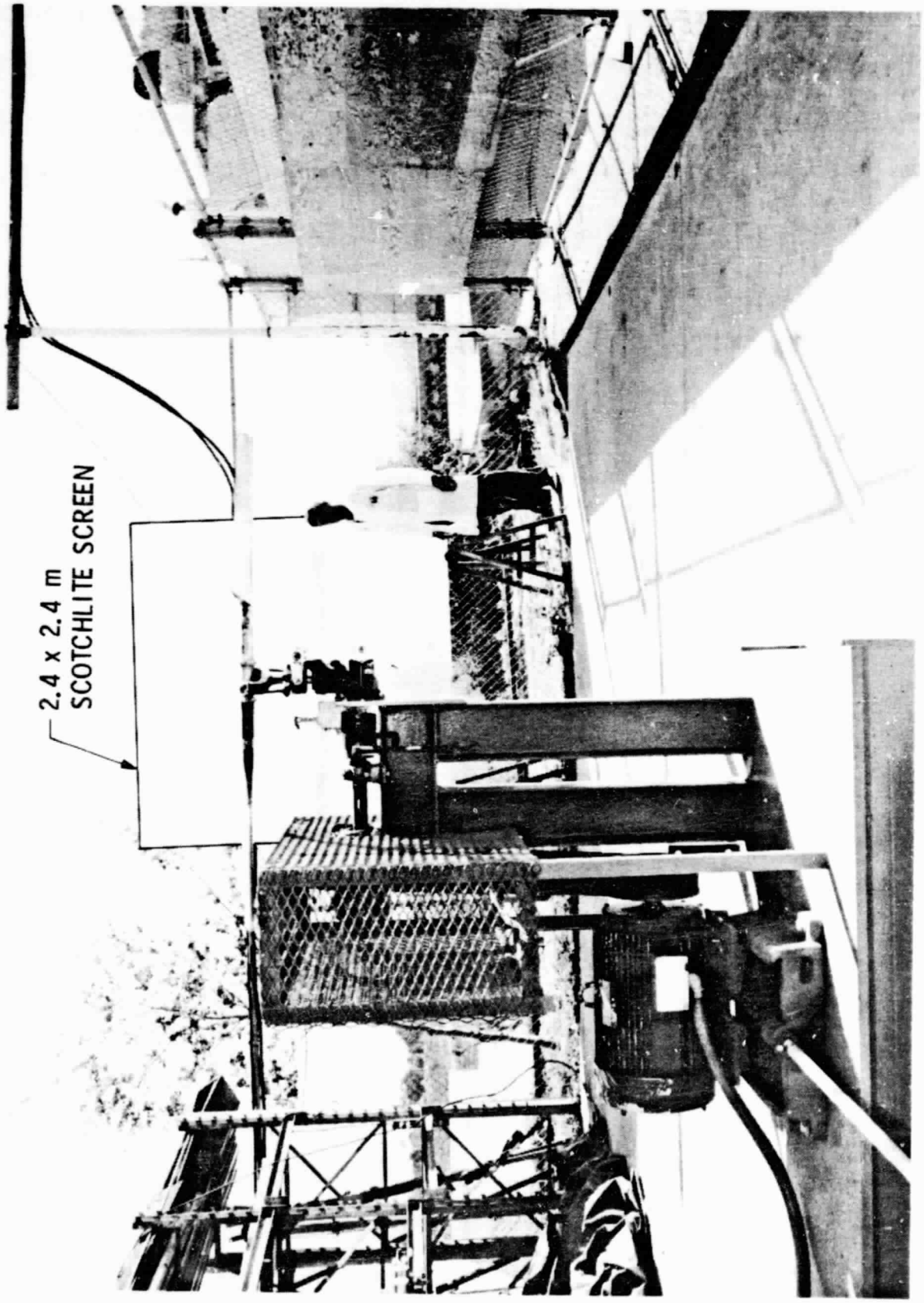

Fig. 2 Tail Rotor, electric motor and 2.4 m x 2.4 m Scotchlite Screen Picture

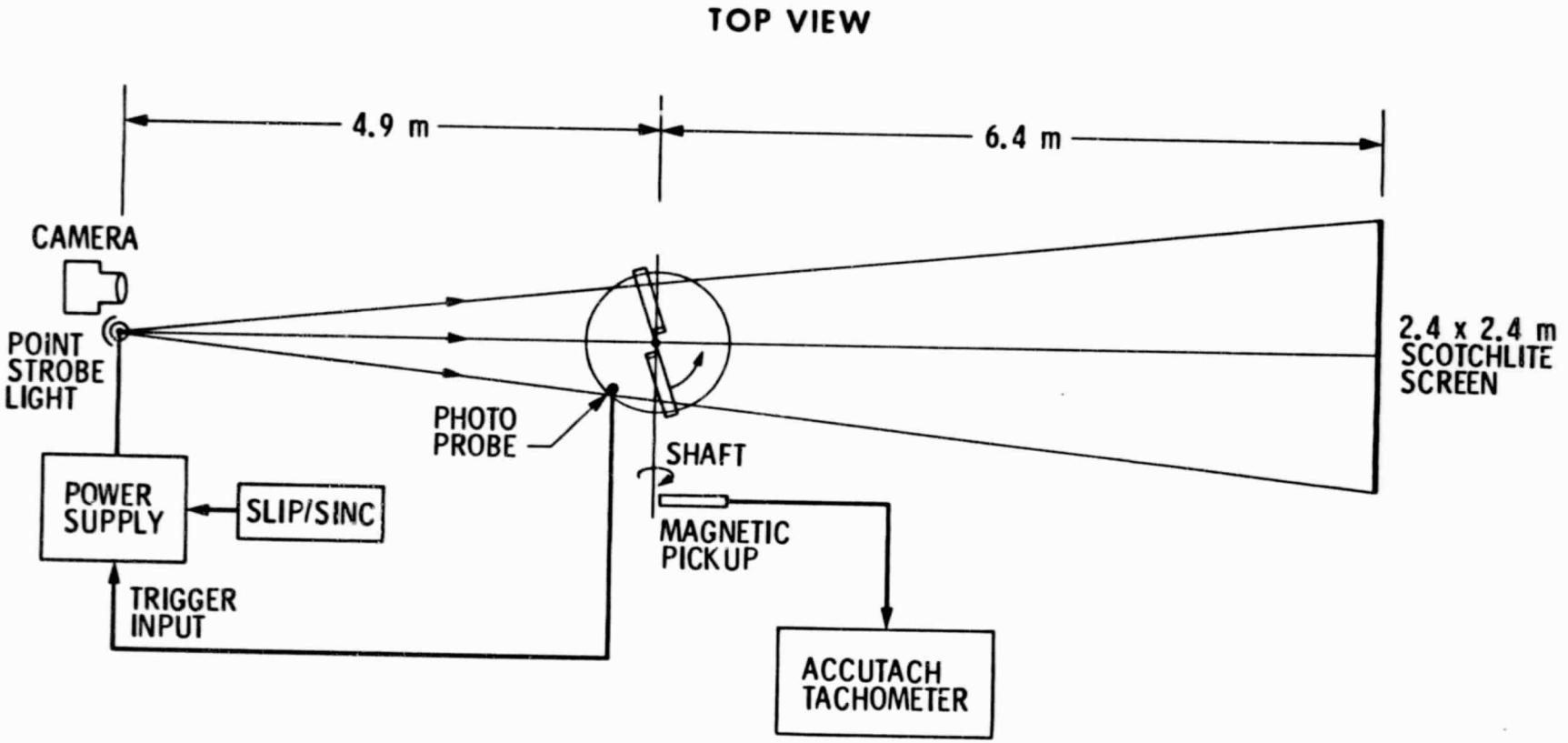

Fig. 3 Sketch of widefield shadowgraph instrumentation.

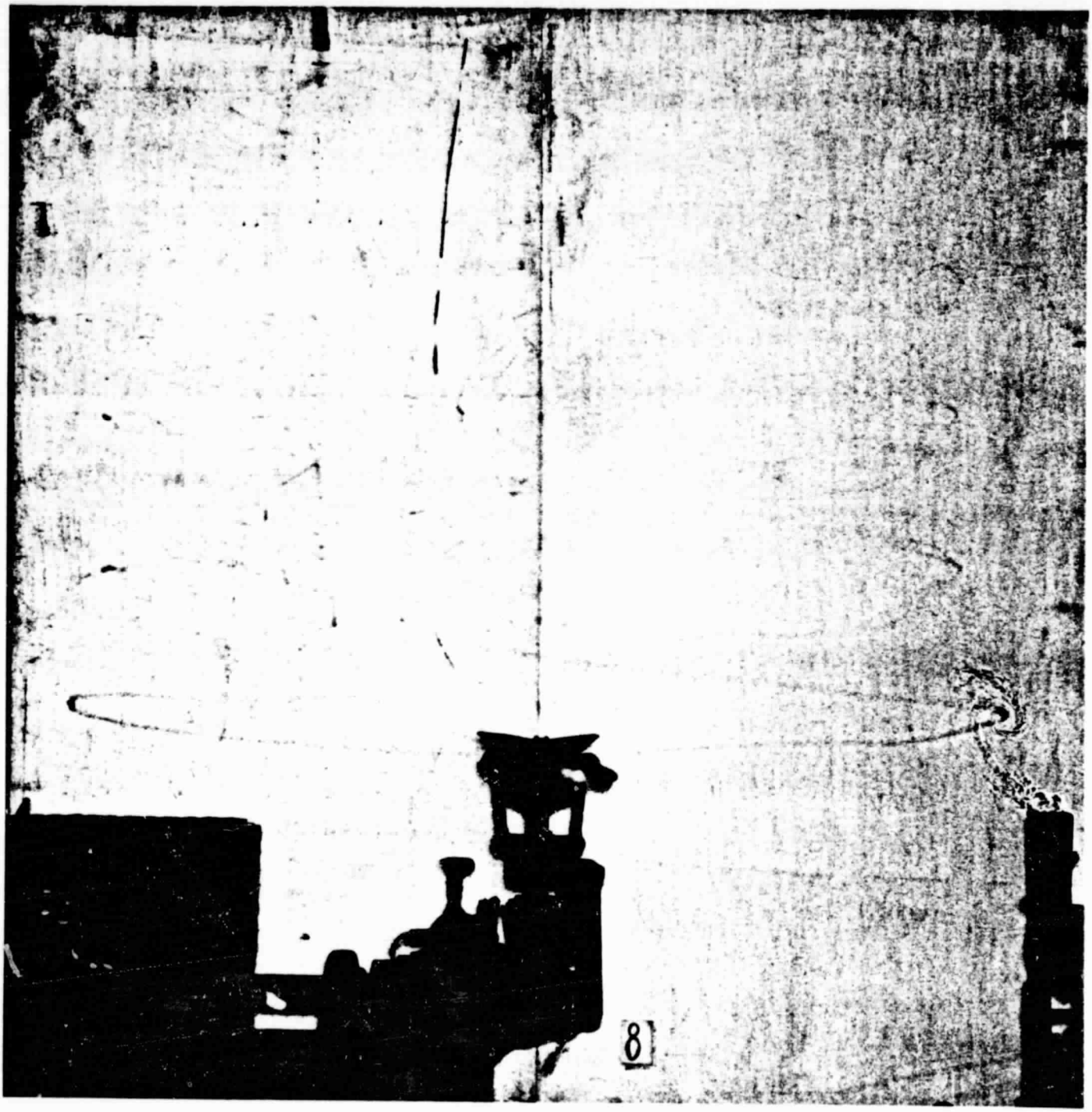

Fig. 4 Shadowgraph Photograph of the Vortex Structure for the Tail Rotor, M_T = 0.64, 3200 rpm, α = 12° ℓ = 4.4 m with heat, Rotor Tip is facing the viewer. Vortex structure is visible.

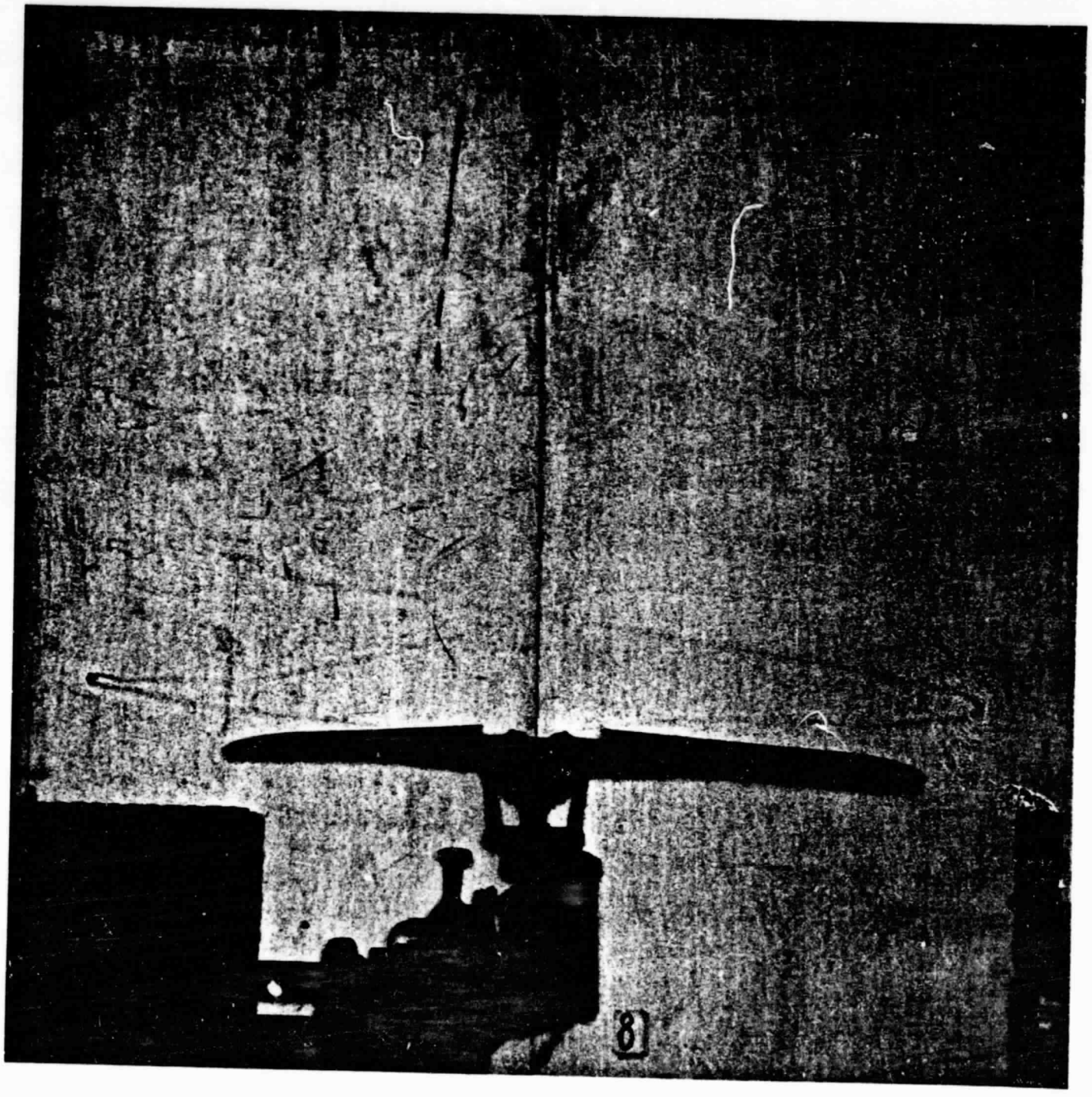

Fig. 5 Shadowgraph Photograph of the Vortex Structure for the Tail Rotor, M_T = 0.64, 3200 rpm, α = 12° ℓ = 4.4 m with heat, Rotor is located normal to the viewer. Vortex structure is visible.

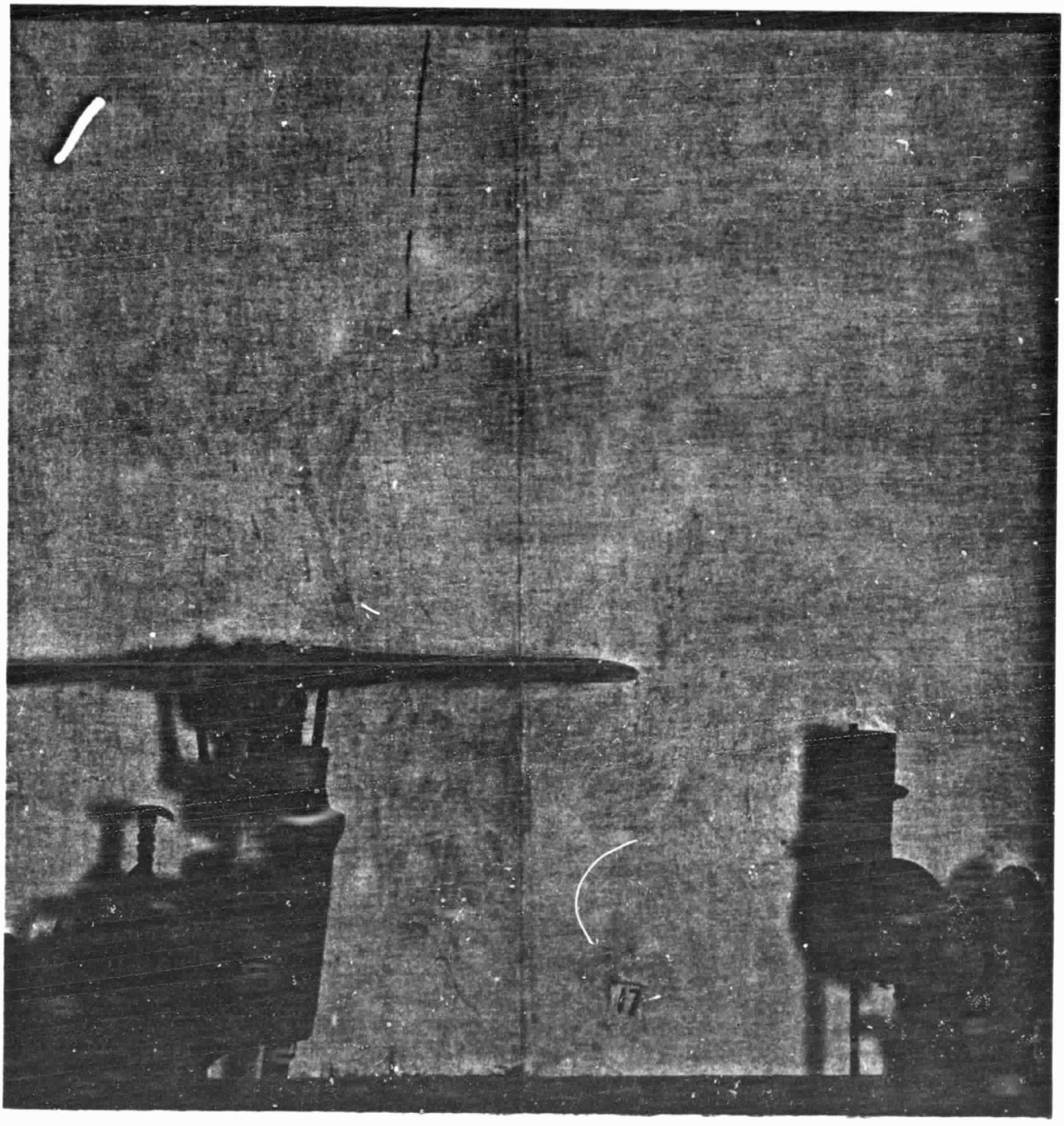

Fig. 6 Shadowgraph Photograph of the Vortex Structure for the Tail Rotor, M_T = 0.38, 1920 rpm, α = 4° ℓ = 6.4 m without heat. Vortex structure is not visible.

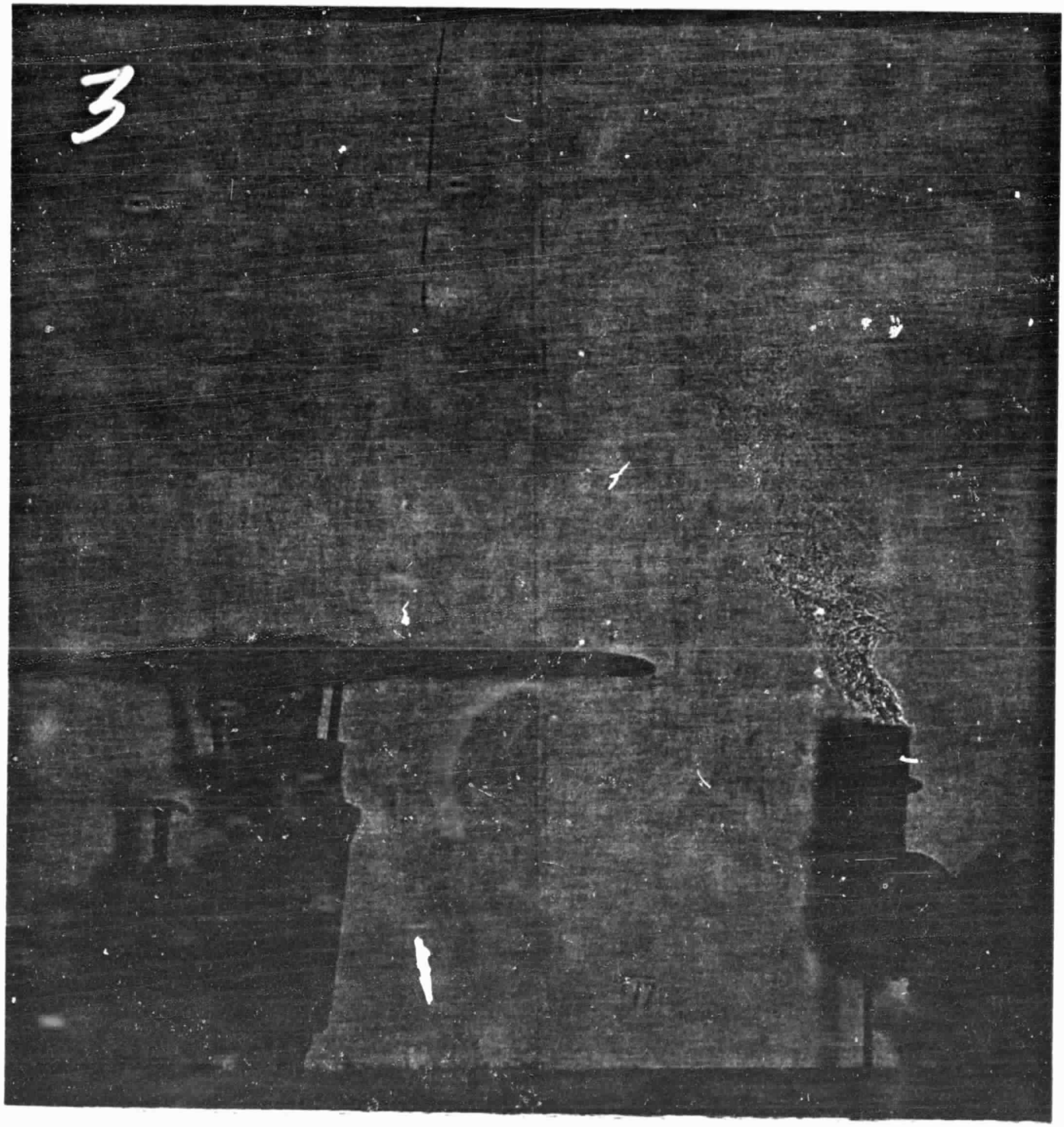

Fig. 7 Shadowgraph Photograph of the Vortex Structure for the Tail Rotor, M_T = 0.38, 1920 rpm, α = 4° ℓ = 6.4 m with heat. Vortex structure is not visible.

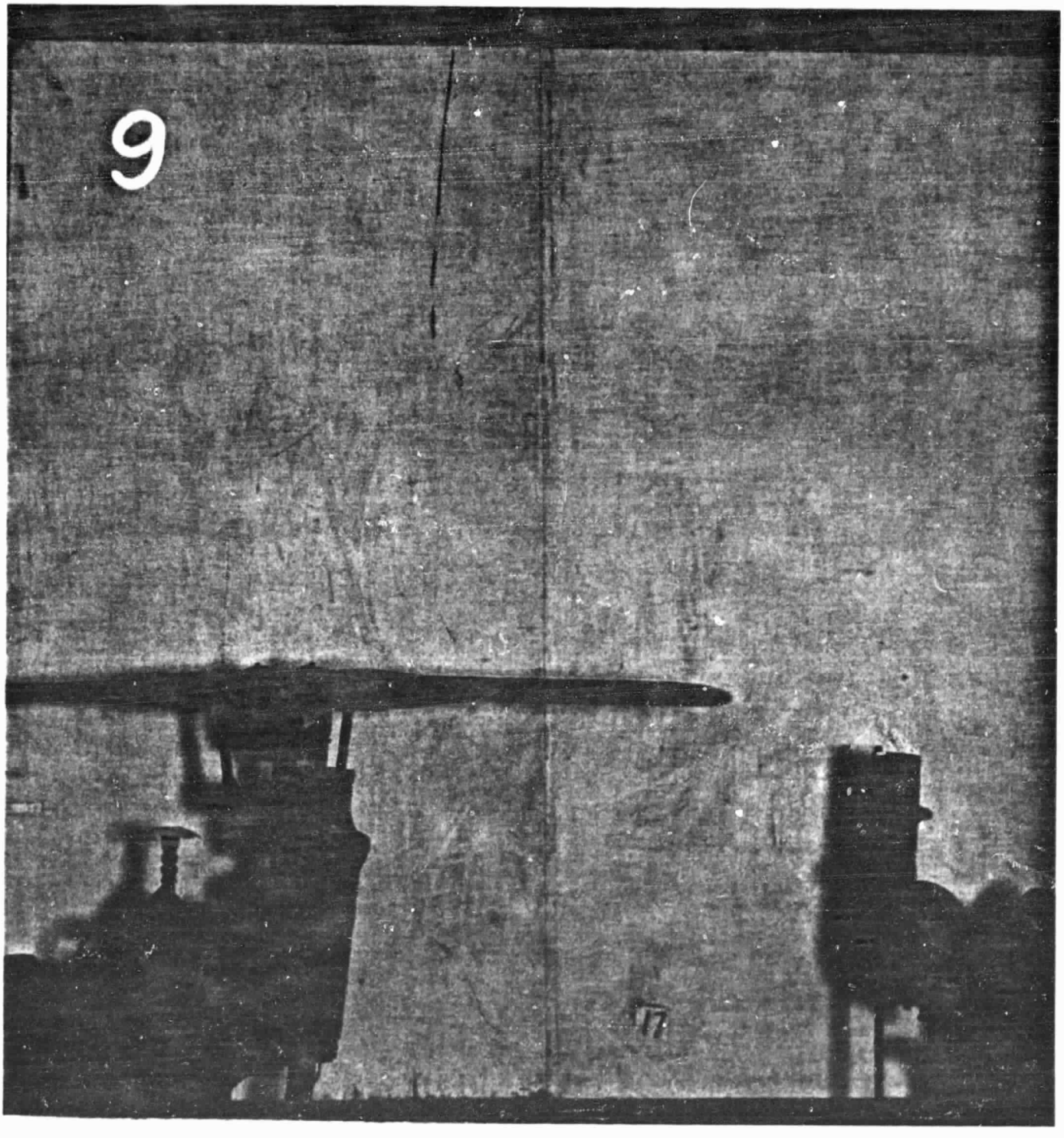

Fig. 8 Shadowgraph Photograph of the Vortex Structure for the Tail Rotor, M_T = 0.55, 2763 rpm, α = 4° ℓ = 6.4 m without heat. Vortex structure is not visible.

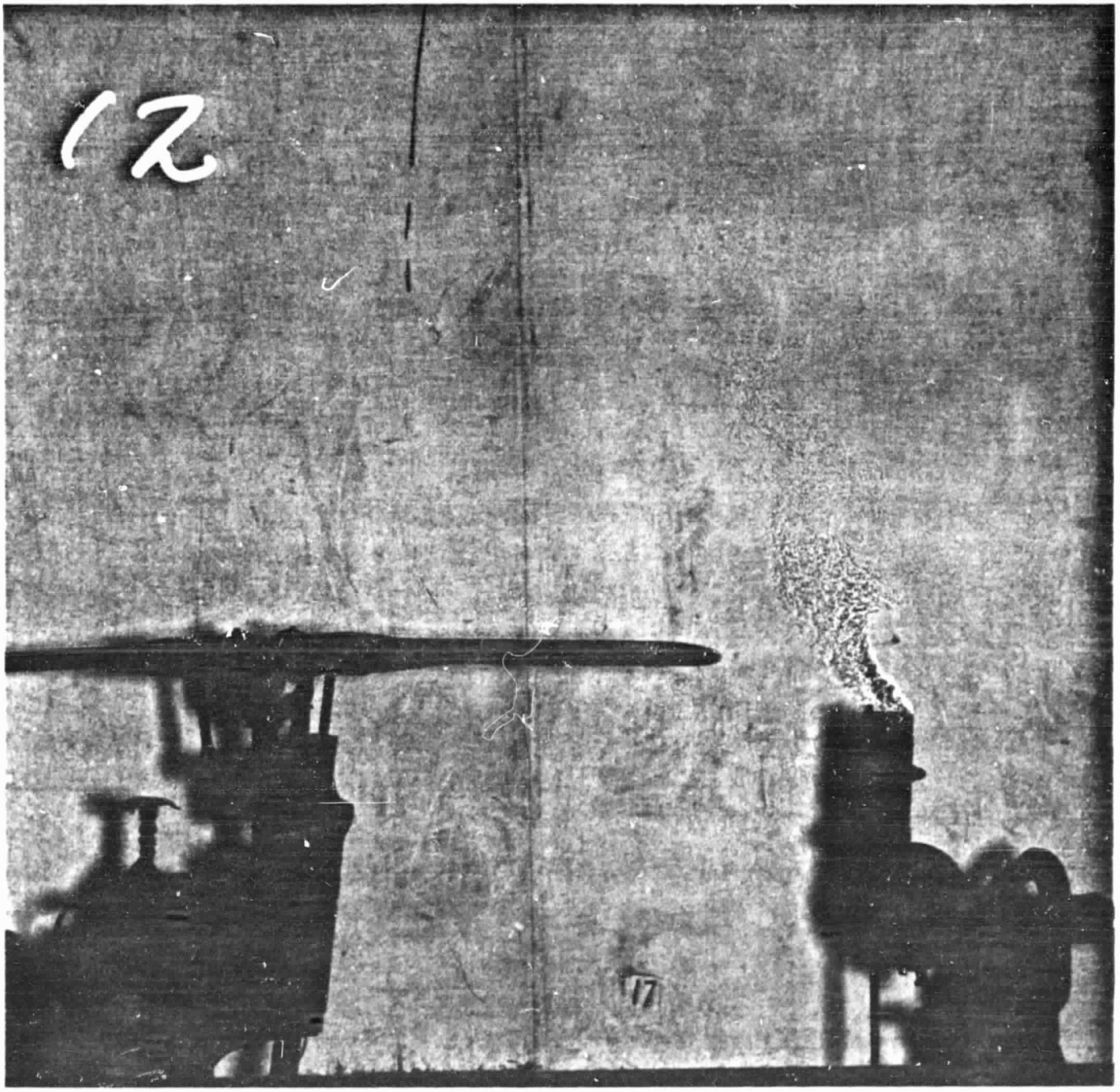

Fig. 9 Shadowgraph Photograph of the Vortex Structure for the Tail Rotor, M_T = 0.55, 2763 rpm, α = 4° ℓ = 6.4 m with heat. Vortex structure is not visible. Vortex structure is visible.

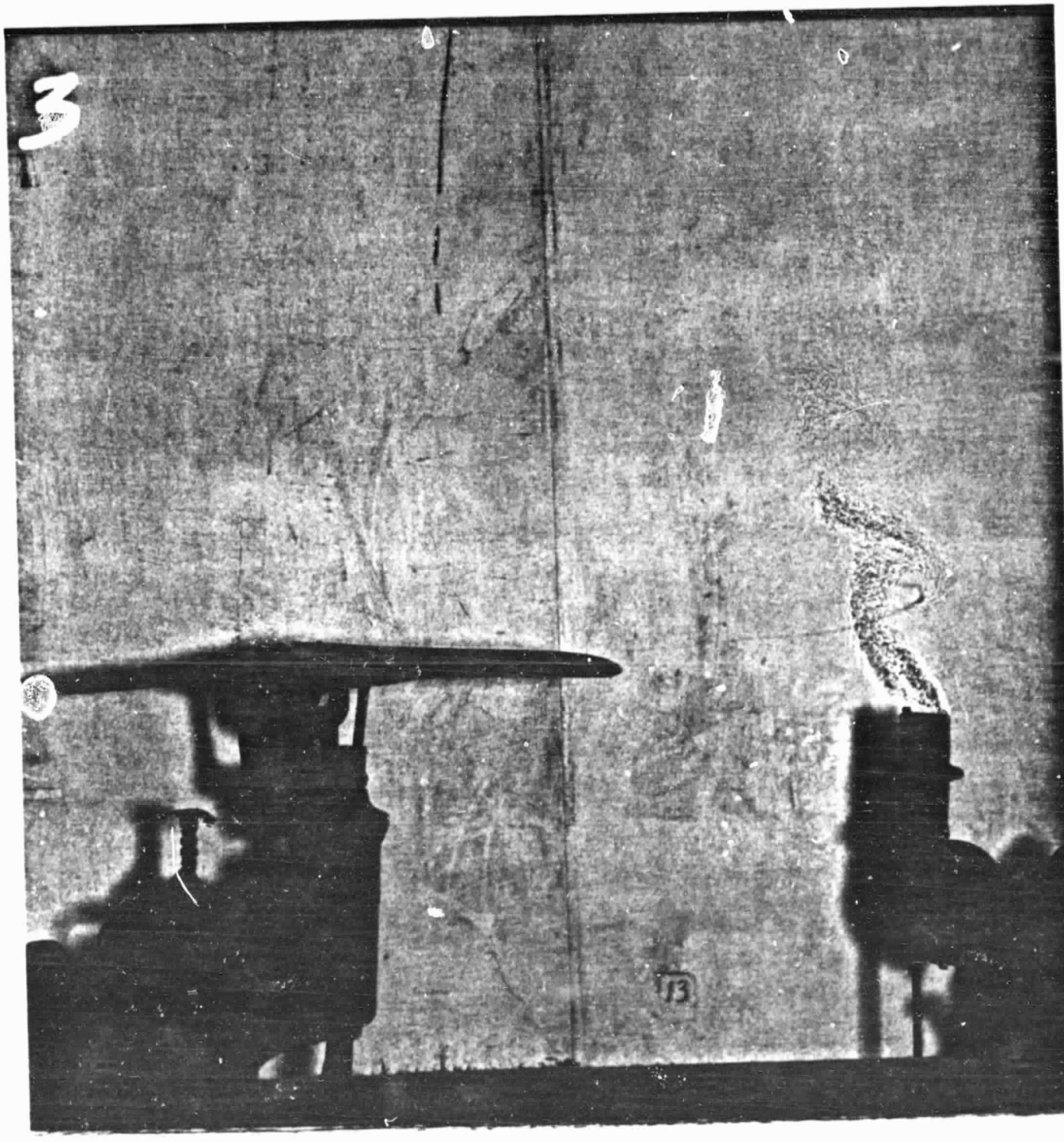

Fig. 10 Shadowgraph Photograph of the Vortex Structure for the Tail Rotor, M_T = 0.38, 1910 rpm, α = 8° ℓ = 6.4 m with heat. Vortex structure is visible.

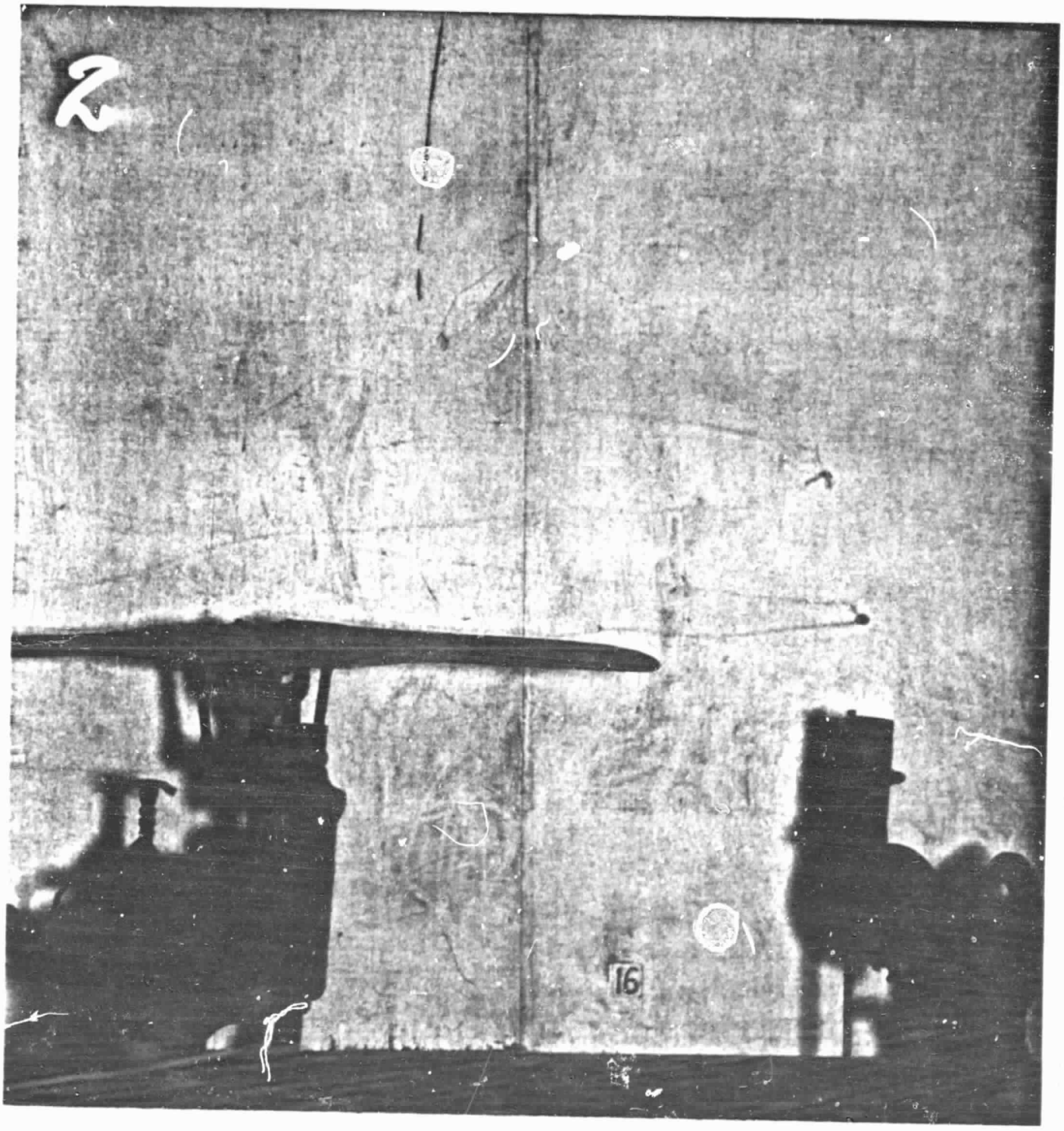

Fig. 11 Shadowgraph Photograph of the Vortex Structure for the Tail Rotor, M_T = 0.58, 2890 rpm, α = 8° ℓ = 6.4 m without heat. Vortex structure is visible.

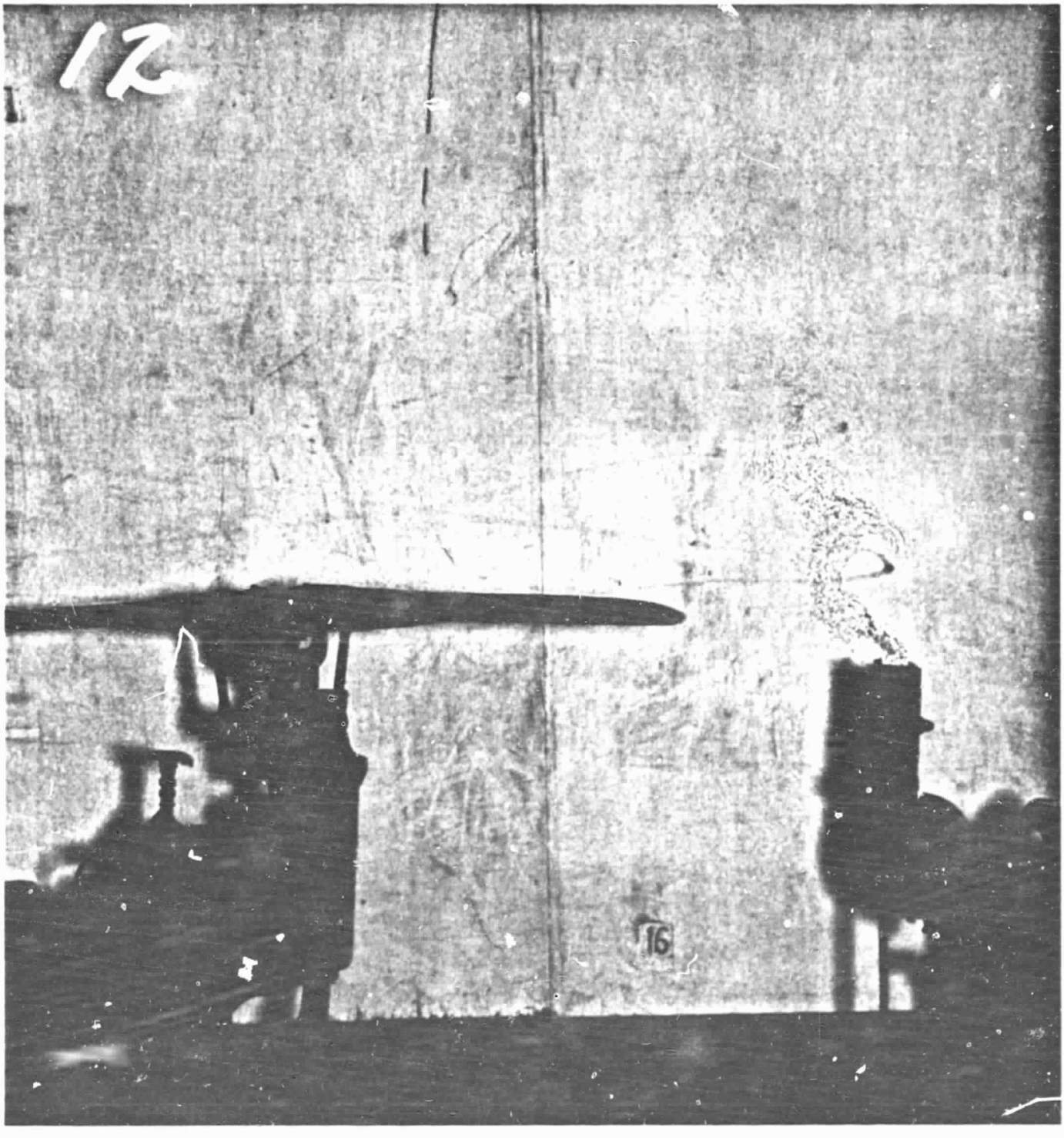

Fig. 12 Shadowgraph Photograph of the Vortex Structure for the Tail Rotor, M_T = 0.58, 2890 rpm, α = 8° ℓ = 6.4 m with heat. Vortex structure is visible.

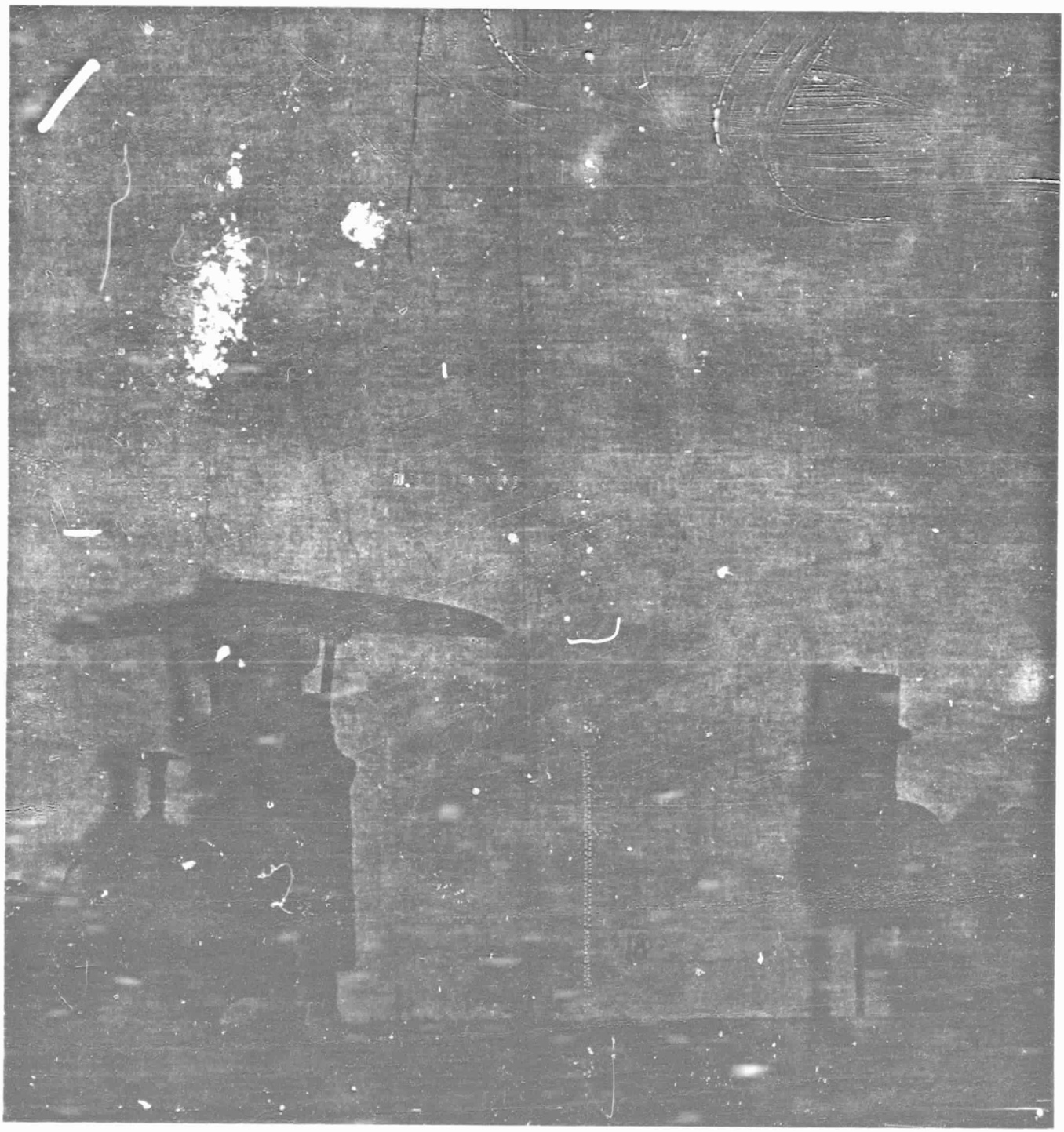

Fig. 13 Shadowgraph Photograph of the Vortex Structure for the Tail Rotor, M_T = 0.38, 1908 rpm, α = 14° ℓ = 6.4 m without heat. Vortex structure is visible.

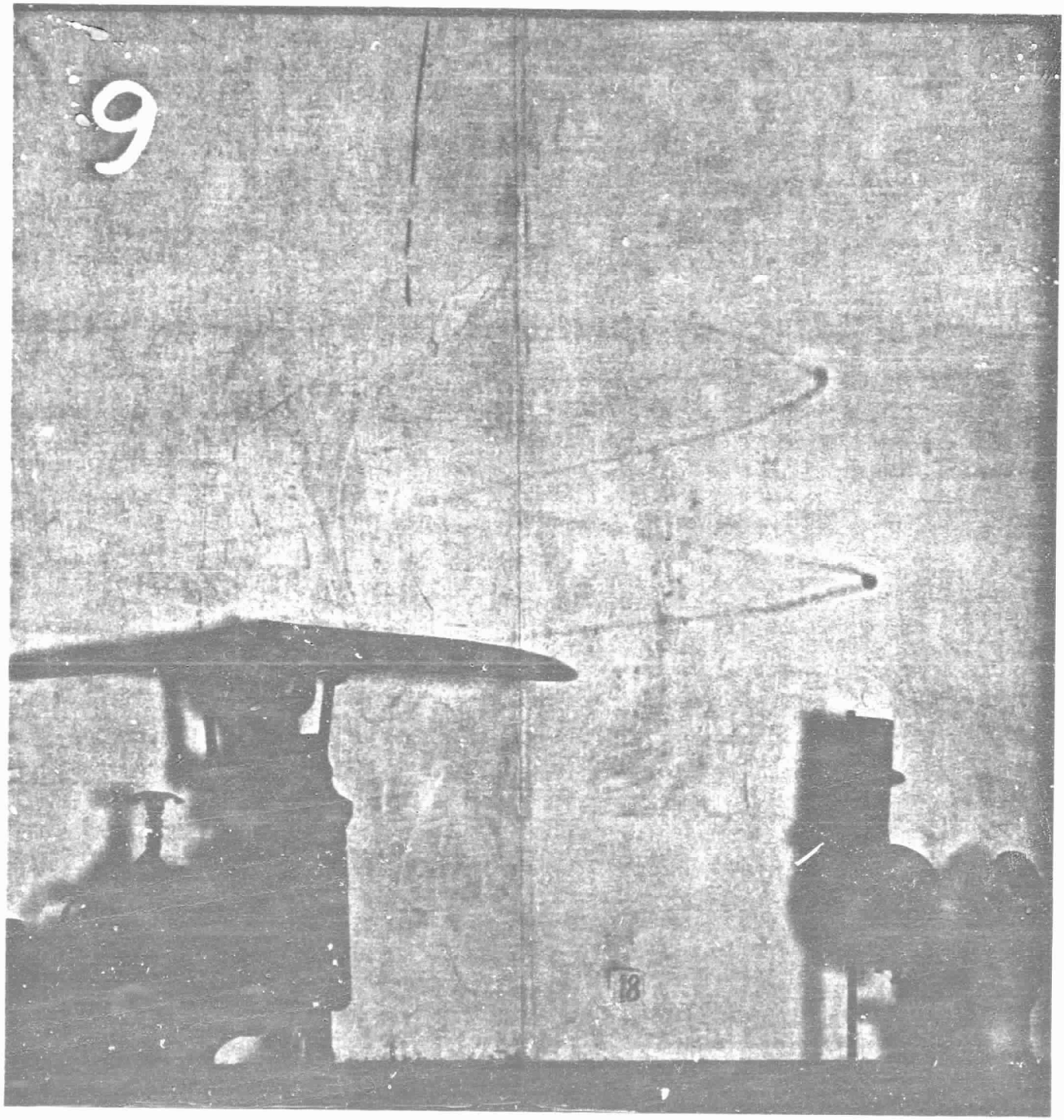

Fig. 14 Shadowgraph Photograph of the Vortex Structure for the Tail Rotor, M_T = 0.38, 1908 rpm, α = 14° ℓ = 6.4 m with heat. Vortex structure is visible.

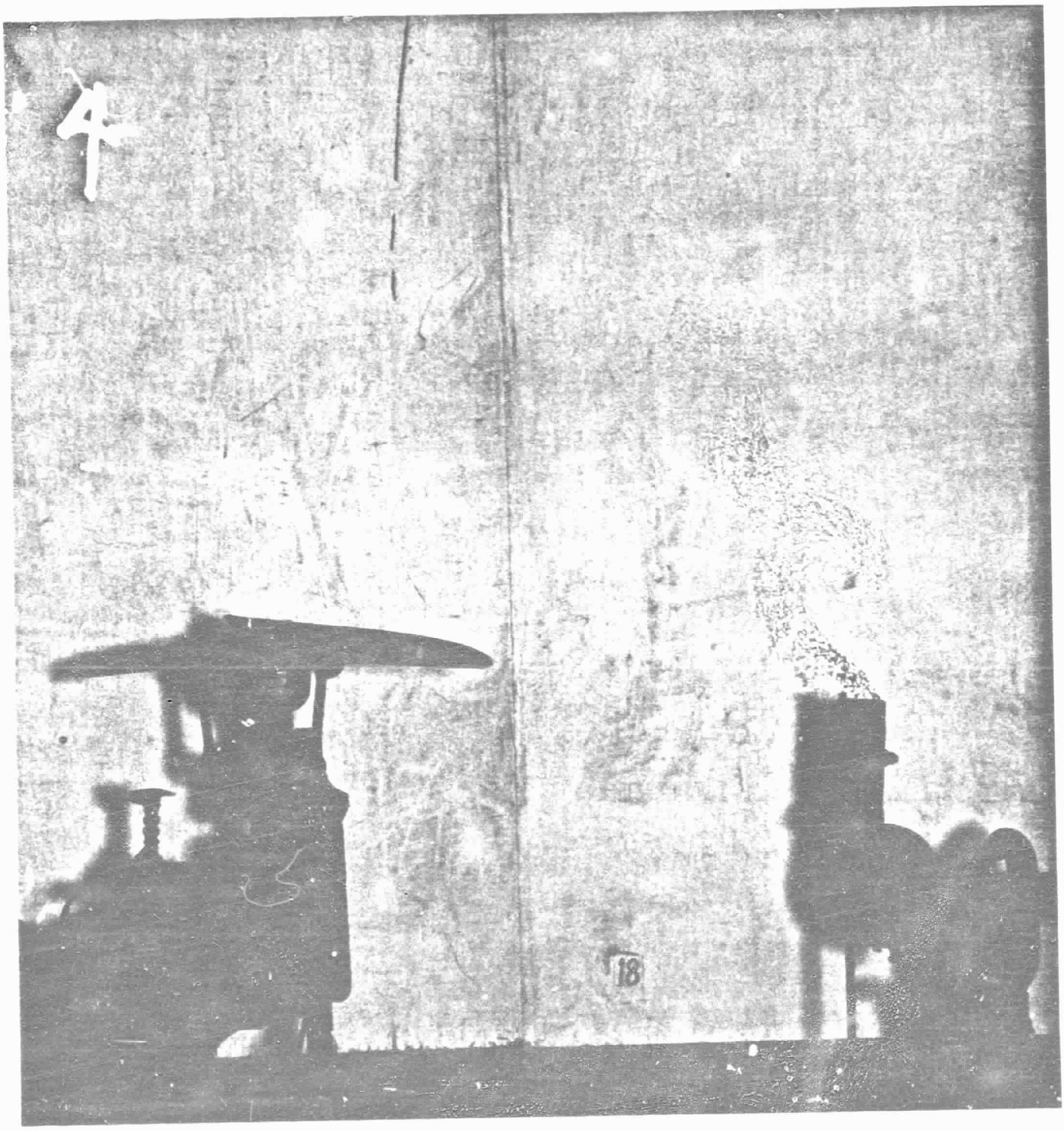

Fig. 15 Shadowgraph Photograph of the Vortex Structure for the Tail Rotor, M_T=0.55, 2762 rpm, α=14° ℓ = 6.4 m without heat. Vortex structure is visible.

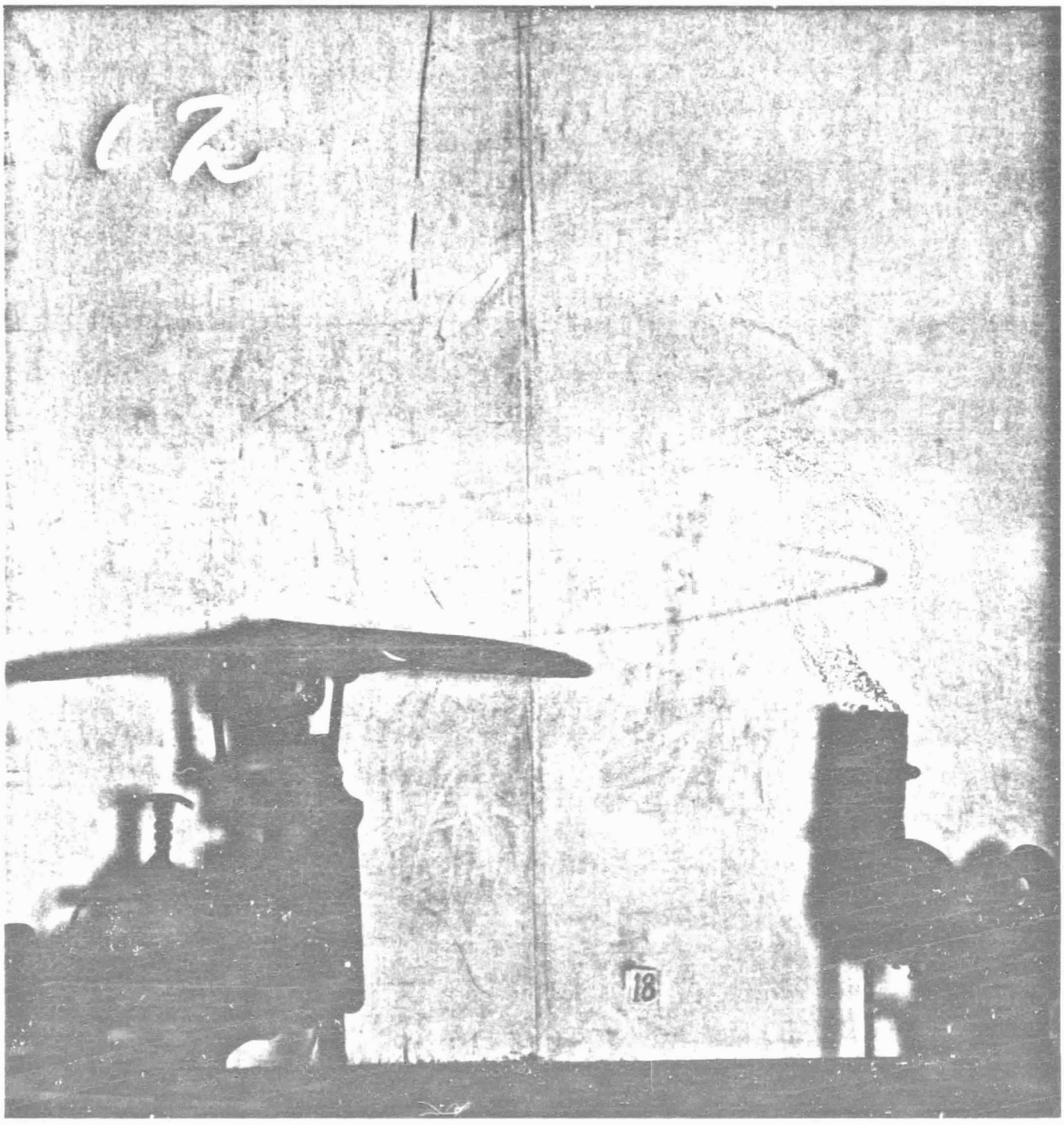

Fig. 16 Shadowgraph Photograph of the Vortex Structure for the Tail Rotor, M_T=0.55, 2762 rpm, α=14° ℓ = 6.4 m with heat. Vortex structure is visible.

APPENDIX

In the Appendix, further data analysis is carried out. Also, an analysis of the visibility function is given.

WIDE-FIELD SHADOWGRAPH FLOW VISUALIZATION OF TIP VORTICES GENERATED BY A HELICOPTER ROTOR+

S.P. Parthasarathy*, Y.I. Cho* and L.H. Back**
Jet Propulsion Laboratory
California Institute of Technology
Pasadena, California

Abstract

The vortex trajectory and vortex wake generated by helicopter rotors were visualized using a wide-field shadowgraph technique. Use of a retro-reflective Scotchlite screen made it possible to investigate the flow field generated by full-scale tail rotors. Tip vortex trajectories were visible in shadowgraphs for a range of tip Mach number of 0.38 ~ 0.60. The effect of the angle of attack was substantial. At an angle of attack greater than 8 degrees, the visibility of the vortex core was significant even at relatively low tip Mach numbers. The theoretical analysis of the visibility was carried out for a rotating blade. This analysis demonstrated that the visibility decreases with increasing dimensionless core radius (r_o/c) and increases with increasing tip Mach number. Based on this investigation, it is concluded that the wide-field shadowgraph flow visualization technique should be feasible to study the flow field generated by a large main rotor in a wind tunnel and in an outdoor full-scale test stand. Of note is that the shadowgraph technique could easily be used with other on-going tests such as aerodynamic performance study, noise measurements, velocity measurements with LDV or hot-wire anemometer, local pressure measurement on the rotor surface, etc.

Nomenclature

A	area of disk
AR	Blade aspect ratio, R_T/c
a_o	ambient speed of sound
b	number of blades
B	factor less than 1 in $v = \Gamma B/2\pi r$
c	blade chord
C_ℓ	section lift coefficient, $L/\frac{1}{2}\rho U^2 c$
C_T	rotor thrust coefficient, $T/\rho\pi R_T^4\Omega^2$
I	intensity
L	lift per unit span ($=\rho\Gamma U$)
ℓ	beam lengths, distance between rotor and screen.
M	Mach number
M_T	tip Mach number
n	refractive index
r	radius measured from the tip vortex center
r_o	core radius of tip vortex
R	radial coordinate along rotor blade
R_T	blade tip radius measured from the hub center
t	time
T	rotor thrust
S	visibility function defined in Eq. (28)
U	free stream velocity in a rectilinear motion or ΩR for rotor blade
U_{max}	maximum free stream velocity in a rectilinear motion
v	circumferential velocity in vortex
W	axial velocity in the far wake
x	coordinate
y	coordinate
z	coordinate
α	angle of attack
β	dimensionless constant in Eq. (22), 0.000292 for air
δ	velocity factor that changes from 0.5 to 1 from the disk to downstream infinity
Γ	circulation ($= 2\pi rv$)
γ	ratio of specific heats (1.4 for air)
υ	kinematic viscosity
ρ	density
σ	rotor solidity, ratio of blade area to rotor disc area ($bc/\pi R_T$)
Ψ_w	wake azimuth angle
Ω	rotor rotational speed
ω	rotational speed in vortex core

I. Introduction

Accurate prediction of the instantaneous flow field and associated performance of a lifting rotor is the key to improve blade designs for helicopters. Over the past thirty years, numerous investigators have attempted to determine rotary-wing inflow and performance using various mathematical methods. Landgrebe and Cheney[1] made an extensive survey of these earlier rotor inflow studies. They divided about eighty references into four categories. These are inflow methods based on 1) momentum theory assuming a uniformly loaded actuator disc without tip loss, 2) undistorted wake geometry neglecting wake contraction, 3) a theoretical distorted wake geometry and 4) prescribed empirical wake geometry.

Concurrent with these analytical and semi-analytical studies, a number of investigators have carried out experiments to better understand wake geometry and corresponding airload of rotors. Detailed blade loading was obtained using hub-mounted pressure transducers[2-4], hot-wire anemometer[4,5], and laser doppler velocimetry[6-8]. Of note is that as pointed out by Yu and Kittleson[9], pressure transducer instrumented airfoils are expensive and difficult to fabricate, and measurements can be made only on the blade surface. Hot-wire anemometry is located within the flowfield, thus disturbing the flow. Furthermore,

+ This paper presents the results of one phase of research carried out by the Jet Propulsion Laboratory, California Institute of Technology, under Contract No. NAS7-918, sponsored by the National Aeronautics and Space Administration, AMES Research Center.
* Member of the Technical Staff, Member AIAA
** Technical Group Supervisor, Associate Fellow, AIAA

both hot-wire anemometry and laser dopper velocimetry are time-consuming point measurements for the complex three-dimensional flow field generated by helicopter rotors. In spite of these difficulties, these methods provided excellent quantitative data on the detailed structure of the flow field of a rotor. Recently, Yu and Kittleson[9] used holographic interferometry and computer assisted tomography to determine the transonic velocity field of a model rotor blade in hover at a tip Mach number of 0.90.

Wake geometry was observed using smoke photography,[10-12], Schlieren technique[13-15], direct observation using the condensation of moisture in the low pressure vortex core[10,16], etc. The smoke injection technique, one of the simplest methods, provided three or four dark vortex cores, thus indicating the wake contraction boundary distinctively. Also, it revealed the presence of the vortex sheet by the discontinuity in smoke streaks. However, this does not provide the vortex spiral trajectory. In addition, the rapid diffusion and the excessive quantity of smoke required pose significant problems in the use of smoke photography for a full scale main rotor test. Schlieren photography is practically restricted to a field of view of about 50 cm because of the necessity of using high quality mirrors in the technique. For this reason, it has been used to visualize the tip vortex trajectory produced by a relatively small model rotor. Direct observation using condensation of moisture is only possible when the humidity and temperature conditions are appropriate and the rotor tip speed is relatively high such that vapor trails are visible. Of note is that these flow visualization techniques provide qualitative two-dimensional views of three-dimensional flow.

However, these techniques produced valuable information on wake geometry such as wake contraction, distortion of wake, nonsymmetry of wake, radial and axial movement of vortex core, which are needed in the analytical prediction of the performance of a lifting rotor. Most investigators studied the wake of a hovering helicopter rotor because of the importance of hovering performance. Also, the hovering condition is the simplest one for experimental set-up.

The objective of the present investigation was to develop a new experimental technique to visualize the helicopter rotor wake to determine the geometry and structure of the tip vortices of a full-scale rotor. The vortices should be observed for several blade passages above the rotor. An important condition in the design of the experiment was to conduct the experiment at nearly full scale (i.e., the distance between the screen and rotor blade should be the order of 3~9 m) so that the system of measurement could apply to a large wind tunnel test.

It was expected that useful shadows would result from the natural density changes in the vortex cores associated with low pressures. However, it was necessary to determine the visibility experimentally since the sensitivity of the shadowgraphs depends on the second derivative of the unknown density field.

Addition of a fluid with different density was also investigated to determine the characteristics of the resulting shadowgraphs. This was done by using a hot air gun during some of the tests.

II. Method of Experiment

Shadowgraphy is the simplest optical technique. Here, second derivatives of density are sensed as light variations on the screen. When a point source illuminates a large screen, density changes in the test section between the light source and the screen cause shadows to be cast on the screen. This shadow can be seen directly or can be photographed by a camera provided there is enough light to produce a good exposure. Usually, light is insufficient for a good exposure if the screens are ordinary, white surfaces.

However, when the screens are treated with retroreflecting material such as Scotchlite (made by 3M company), the light gathered by a camera placed as close as possible to the point source of light is sufficient for a good exposure. A stroboscope is generally used to freeze the motion during the time the camera shutter is open.

Shadowgraphy reveals naturally occuring density changes in the flow as well as those changes induced by deliberate introduction of tracers of different densities such as hot air, carbon dioxide gas, etc. In the present application, tip vortices from rotors cause enough density changes to be visible without the introduction of tracers. However, tracers can be used to examine the flow field in regions where there are no naturally occuring density changes.

To simulate flow fields generated by rotorcraft blades, a tail rotor together with the gear box (Hughes Model 300) was obtained through the Sheriff's Department, County of Los Angeles. The symmetric blade was rectangular with chord length of 0.122 m (NACA airfoil 0015). The distance from the center of rotation to the blade tip was 0.65 m giving the blade aspect ratio (AR) of 5.3 and the rotor solidity (σ) of 0.120. The designed-operating speed of this rotor was 2900~3100 rpm with a torque of 269 N-m. At 3100 rpm, the blade tip speed was 210 m/s (i.e., Mach number 0.61) and the required electric motor power to rotate the rotor was 18.6 Hp.

The rotor test assembly was balanced with the Vibrex Track and Balance System made by the

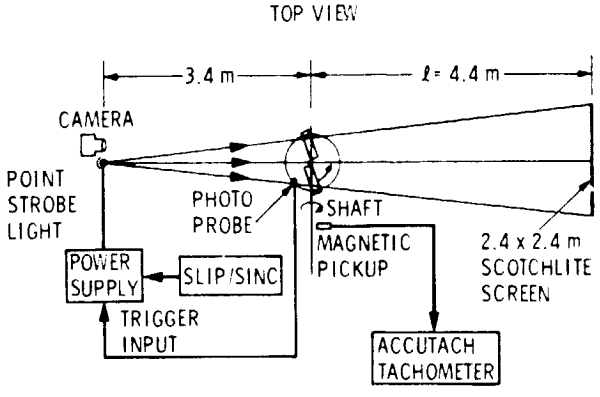

Fig. 1 Sketch of widefield shadowgraph instrumentation.

Chadwick and Helmuth Company (El Monte, CA). During the balancing test, the maximum operational speed of 3100 rpm was obtained.

The setup with camera focused on the shadow on the Scotchlite screen is shown in Fig. 1. The aperture (f) of 5.6 and shutter speed of 1/15 sec. were used to take the shadow photographs with Kodak film (Tri-X PAN 120, ASA 400). Stroboscopic observations were made by syncronizing the Xenon point-source strobe lamp with the signal from the photoprobe, thus automatically freezing the rotor blade motion at a fixed location throughout the test. A typical flash rate during photography was 25 flash/sec with a pulse power of 2.88 J/flash. Each flash duration was 21 μs. In addition, the use of slip/sinc control in the Strobex System (made by the Chadwick and Helmuth Company) allowed us to observe transient shadowgraphs from slowly moving rotor blades. The magnetic pickup probe mounted near the shaft connecting the rotor clutch device to the electric motor measured the shaft rpm which was 2/3 of the rotation speed of the rotor because of the gear ratio used in the device. The rpm measured using the magnetic sensor was the same as the stroboscopically measured data within five percent. Scotchlite shadowgraphs were observed at two distances, viz ℓ = 4.4 m between the rotor and screen and also ℓ = 6.4 m. The corresponding distances between the light source and screen were 7.8 m and 11.0 m, respectively. These distances could be expected in applications of this technique when the strobe source is located in a large wind tunnel.

III. Experimental Results and Discussion

Figure 2 shows the shadowgraph of the rotor at ℓ = 4.4 m at 3200 rpm (i.e., M_T= 0.64) and at 12° angle of attack. Of note is that the rotor tip is facing toward the viewer. The vortex cores are seen as two thin spirals emanating from the two blade tips. On the left, only the density gradient occurring naturally in the core makes the vortex visible. On the right, hot air from a hair dryer circulates around the tip vortex and shows the circulating flow. At the extreme right and left edges, the shadows are denser because the light rays pass tangentially through the vortices. Three dark spots are visible on the left vertically showing these edges. The vortices are distorted at this condition of high angle of attack and high rpm.

Figure 3 shows another phase of the rotor at the same conditions. Distortions are clearly visible on the left. It is worth noting that these shadowgraph pictures give detailed information on the entire vortex trajectory, the vortex core size and the wake around the vortex core, which can provide useful input for the computer modeling of the helicopter rotor performance[17].

Figure 4 shows the shadowgraph of the rotor at ℓ = 6.4 m, 2890 rpm (i.e., M_T = 0.58) and at 8° angle of attack. Spiralling vortices are distinctly visible and the flow field around two tip vortex cores is dramatically shown with the help of hot air introduced below the rotor tip. By comparing Fig. 4 with Figs. 2 and 3, the shadowgraph picture taken at ℓ = 6.4 m was found to be equally good as (or no better than) those taken at ℓ = 4.4 m, when ℓ is the order of 4 to 6 m.

Other shadow photographs taken at different Mach numbers and different angle of attacks are given in our earlier report[18]. Of note is that for α=4° and ℓ=6.4 m, a just visible tip vortex core was observed at M_T of 0.38, and slightly visible spiralling vortex trajectories together with distinctively visible one dark vortex core spot

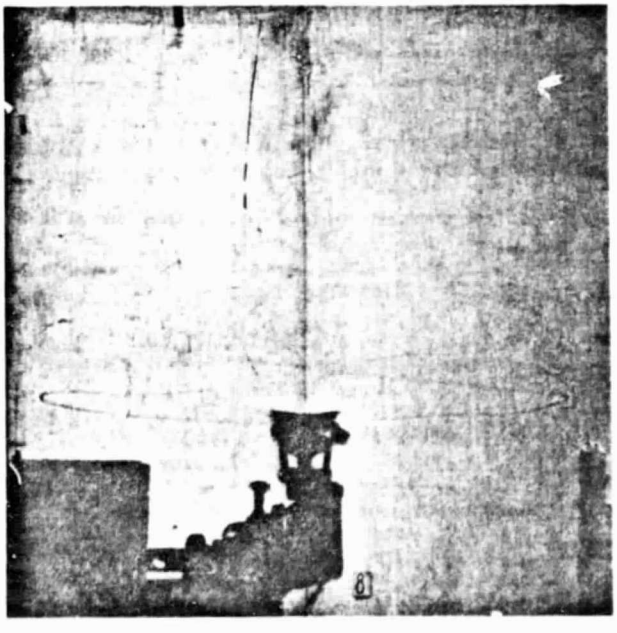

Fig. 2 Shadowgraph Photograph of the Vortex Structure for the Tail Rotor, M_T=0.64, 3200 rpm, α=12° ℓ = 4.4 m with heat. Rotor Tip is facing the viewer. Vortex structure is visible.

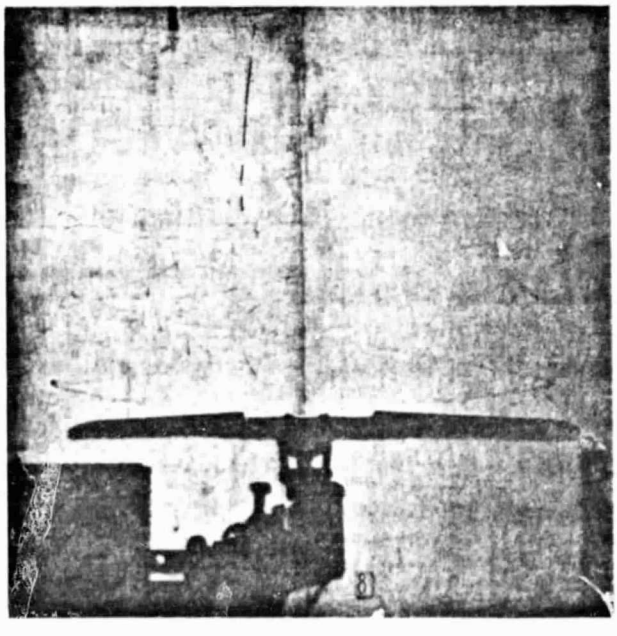

Fig. 3 Shadowgraph Photograph of the Vortex Structure for the Tail Rotor, M_T=0.64, 3200 rpm, α=12° ℓ = 4.4 m with heat. Rotor is located normal to the viewer. Vortex structure is visible.

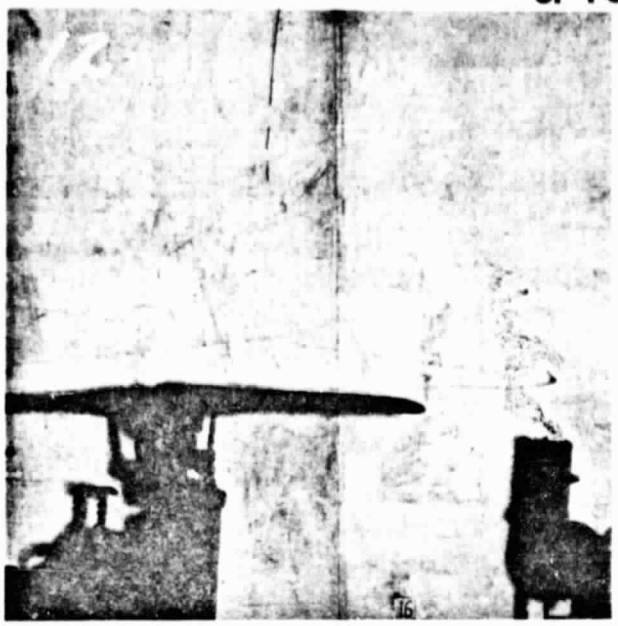

Fig. 4 Shadowgraph Photograph of the Vortex Structure for the Tail Rotor, M_T=0.58, 2890 rpm, α=8° ℓ = 6.4 m with heat. Vortex structure is visible.

were seen at M_T of 0.55. Therefore, the threshold values of α and M_T for the shadowgraphy technique to yield useful information were found to be 4° and 0.38, respectively. In general, visibility significantly improved with the tip speed and angle of attack. However, the effect of the angle of attack α was found to be more important than the tip speed. At an angle of attack greater than 8°, the visibility was significant even at relatively low tip Mach numbers of 0.38 (see shadowgraph pictures in Ref. 18). In the following, it will be demonstrated that three important quantitative data such as vortex core radius r_o, axial velocity in the wake W, and tip vortex axial and radial coordinates, can be obtained from a qualitative shadowgraph flow visualization picture.

a. Vortex Core Radius r_o

The size of the vortex core was experimentally determined from the shadowgraph picture given in Fig. 3 (i.e., α = 12° and M_T = 0.64). Since the rotor radius is 0.65 m, one can calculate the scale-up factor between the real size and shadowgraph image. This results in a value of the vortex core radius of 7.6 mm for the case shown in Fig. 3. Thus, the ratio of the vortex core radius to the chord r_o/c is 0.063.

b. Axial Velocity in the Wake

Shadowgraph pictures in Figs. 2-4 show, typically, two or three vortex cores (for example, see three dark spots at the left side in Fig. 2). Thus, by knowing the rpm and the distance between two vortex cores, one can calculate the axial velocity due to the hovering motion of rotors. For the case of 3200 rpm and an angle of attack of 12° in Fig. 2, the axial velocity was calculated to be 20.4 m/s.

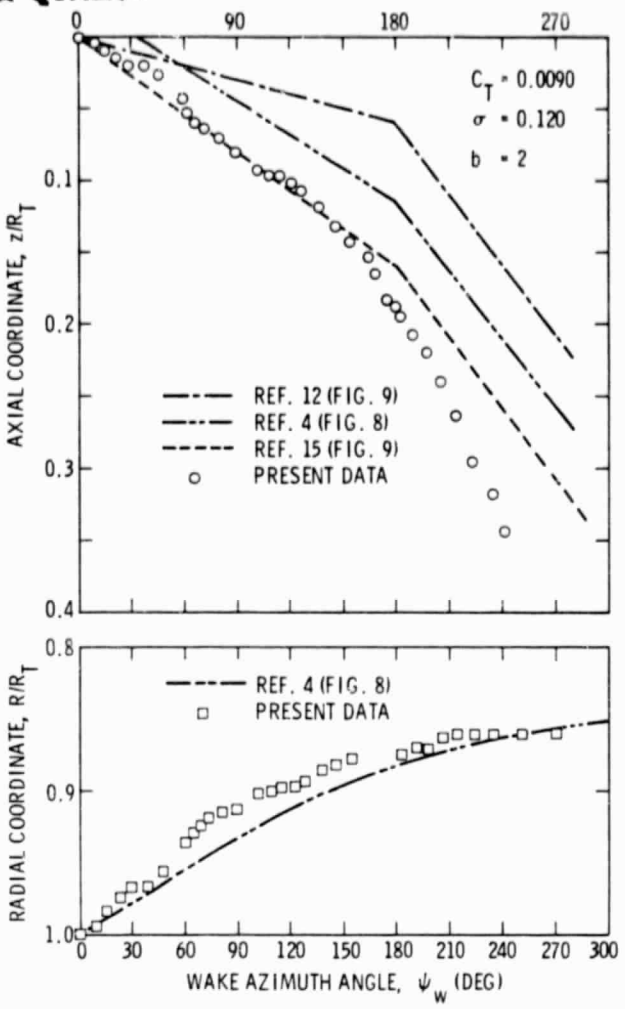

Fig. 5 Axial and Radial Tip Vortex Coordinates vs. Wake Azimuth Angle, Ψ_w.

c. Tip Vortex Coordinates

Axial and radial movements of tip vortices are calculated from the shadowgraph picture given in Fig. 2. In Fig. 2, the angle of attack was 12° at 3200 rpm (i.e., M_T = 0.64). The data reduction procedure was similar to those used by Landgrebe[12,17] and Kocurek and Tangler,[15] and results are given in Fig. 5, which also shows earlier results obtained by other investigators. Table 1 gives pertinent information on these investigations. Of note is that Landgrebe[12,17] used smoke photography, Kocurek and Tangler[15] Schlieren method, and Caradona and Tung[4] hot-wire anenometer probe to obtain the tip vortex coordinates. In addition, Landgrebe's, and Kocurek and Tangler's data were read from their wake-fitting formula correlated in terms of C_T/σ and C_T respectively, while Cardona and Tung's data were read at a given pitch angle. Of note is that all the above-mentioned investigators used an airfoil type NACA 0012. In the present study, C_T was not measured experimentally. However, by knowing the blade shape (i.e., NACA 0015) and angle of attack (i.e., 12°), one can calculate the average lift coefficient C_ℓ and accordingly the thrust coefficient C_T from $C_T = bC_\ell/(6\pi AR)$. Values of C_ℓ and C_T were 0.45 (i.e., see Ref. 4) and 0.0090 respectively, for the present case given in Fig. 2.

The results of Kocurek and Tangler[15] who used a Schlieren method are in relatively good agreement with our shadowgraph technique at wake azimuthal angles to about 100 deg, but at larger angles do indicate smaller axial displacement of the tip vortex. The other techniques of Caradona and Tung,[4] and Landgrebe[12,17] give progressively smaller axial displacements. Kocurek and Tangler[15] have pointed out differences between their results and those of Landgrebe for tip vortex axial position in terms of the blade aspect ratio AR and number of blades b. Our results for one aspect ratio AR = 5.3 and 2 blades appear to be similar to those of Kocurek and Tangler with 2 blades, although somewhat larger tip vortex axial locations are indicated than for the similar rotor results of Caradona and Tung (AR = 6 and b = 2).

Figure 5 clearly demonstrates that the shadowgraphy technique can be used to measure tip vortex axial and radial coordinates. The present data reveals non-linearity of the axial coordinate of tip vortices.

IV. ANALYSIS

a. Visibility of a Vortex Wake

A simplified analysis is developed to estimate the influence of angle of attack, and tip speed on the visibility of vortices in the shadowgraphs. More elaborate treatments of trailing vortices have been conducted by many investigators for fixed wings. Large scale vortices from aircraft have been studied by McCormick et al[19]. Simulation of the wake of a large aircraft by a small scale model is discussed by Bate[20]. Growth of vortices in turbulent flow was discussed by Squire[21] by using a suitable eddy viscosity model. Wind tunnel investigations of the far-field wake structure were conducted by Mason and Marchman[22] and the structure of the vortex was related to the circulation distribution on the wing.

b. Rectilinear Motion

Consider first an airfoil in rectilinear motion with velocity U. The airfoil is considered as a lifting line. The vortex has a region of linearly increasing circumferential velocity near the center reaching a maximum value in a transition region followed by a decay as r^{-1} at large distances corresponding to free vortex behavior. The sketch in Fig. 6 shows this distribution.

In Fig. 6, the maximum circumferential velocity is given by

$$v_{max} = \frac{B\Gamma}{2\pi r_0} \tag{1}$$

where the quantity B is to be obtained from vortex theory or from experiments of Corsiglia et al.[23] For a laminar vortex, diffusion of vorticity from a line source gives the solution of the circumferential velocity v (see Lamb[24]);

$$v = \frac{\Gamma}{2\pi r}\left(1-e^{-r^2/4\nu t}\right) \tag{2}$$

which has a maximum at $r = r_0$ where $dv/dr = 0$.

From this, we have $r_0^2/4\nu t = 1.256$. The core radius r_0 increases as the square root of νt as in all diffusion problems. In a steady flow problem, time t is replaced by x/U by Taylor's hypothesis. The maximum circumferential velocity is given by

$$v_{max} = \frac{\Gamma}{2\pi r_0}\left(1-e^{-1.256}\right) \tag{3}$$

$$= 0.715\left(\frac{\Gamma}{2\pi r_0}\right) \tag{4}$$

therefore, for a laminar vortex, the corresponding factor B in Eq. (1) is 0.715.

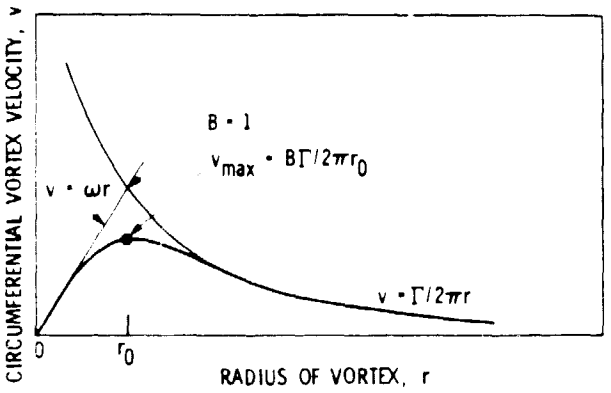

Fig. 6 Velocity distribution in the tip vortex

Flow in a turbulent trailing vortex is discussed by Govindaraju and Saffman[25] where it is shown that the circulation must develop an overshoot. The logarithmic profile of Hoffman and Joubert[26] is explained and previous results of model and flight tests are discussed.

Turbulent vortices, described in terms of core, log region and outer defect region, in analogy with turbulent boundary layers by Hoffman and Joubert, have been further discussed by Corsiglia et al[23] who made measurements with a rapid scanning flying hot wire. From these measurements, the factor B, corresponding to the turbulent trailing vortex, is found to be about 0.42. Thus, the uncertainty involving the constant B in Eq. (1) varies from 0.715 for the laminar vortex to 0.42 for the turbulent one.

Now, for the analysis of the visibility of a vortex wake, a relationship will be developed in the following, which includes the maximum circumferential vortex velocity v_{max}, and velocity U. This relation will be used in the calculation of the density changes due to the flow velocities.

First, the ratio of the circumferential vortex velocity to the free stream velocity, v/U can be given in terms of the circulation Γ by

$$\frac{v}{U} = \left(\frac{\Gamma B}{2\pi r}\right)\cdot\frac{1}{U} \tag{5}$$

Since the lift per unit span L is $\rho\Gamma U$, we have

$$\frac{v}{U} = \frac{LB}{4\pi r(\frac{1}{2}\rho U^2)} \qquad (6)$$

Introducing the lift coefficient C_ℓ, Eq. (6) becomes

$$\frac{v}{U} = \frac{B.C_\ell}{4\pi(r/c)} \qquad (7)$$

where $C_\ell = \frac{L}{\frac{1}{2}\rho U^2 \cdot c}$ (8)

and c is the chord length of the blade.

Since the maximum circumferential velocity occurs at $r=r_o$, Eq. (7) becomes

$$\frac{v_{max}}{U} = \frac{B.C_\ell}{4\pi(r_o/c)} \qquad (9)$$

Applying the B value corresponding to the turbulent trailing vortex, i.e., B = 0.42, we have

$$\frac{v_{max}}{U} = \frac{0.42\ C_\ell}{4\pi(r_o/c)} \qquad (10)$$

For the NACA airfoil 0015 with 12 degree angle of attack in rectilinear motion[27], C_ℓ = 1.11. Thus, using r_o/c = 0.063 which was obtained from our flow visualization pictures, Eq. (10) becomes

$$\frac{v_{max}}{U} = 0.58 \qquad (11)$$

Of note is that the ratio of the vortex core radius to the chord, r_o/c was experimentally found to be 0.053 by Corsiglia, et al[23], who used two geometrically similar fixed wing models (NACA airfoil 0015) with a span of 0.81 and 2.43 m and an aspect ratio of 5.33. Also note that for a laminar vortex (i.e., B=0.715), the value of v_{max}/U in Eq. (11) becomes 1.002.

Equation (11) demonstrates that the maximum circumferential velocity v_{max} is approximately half the airfoil velocity. Such velocity changes are accompanied by significant density changes as will be shown later.

c. Rotating Blade

For a rotor, the flow field is different in the wake because the tip vortices caused by a hovering rotor are surrounded by a smaller axial jet flow. This flow can be calculated following the actuator disk theory as described in Prandtl.[28] The rotor disk increases the velocity of the fluid at the disk by one-half the axial jet velocity far downstream.

The thrust of the rotor T is given in Prandtl[28] which for a hovering rotor is

$$T = \frac{\rho W^2}{2} \cdot (\pi R_T^2), \qquad (12)$$

where W is the axial velocity in the far wake, and the disc area is (πR_T^2) (see Fig. 7).

However, the thrust of the rotor blade can be also expressed by the integration of the differential lift over the entire span of the blade.

$$T = b \int_0^{R_T} L\,dR \qquad (13)$$

Substituting Eq. (8) for L and using $U = \Omega R$, we have

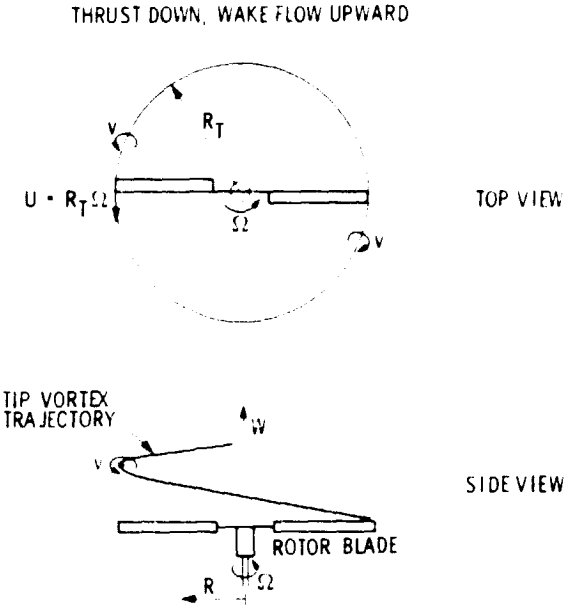

Fig. 7 Sketch of top and side views of two rotors and vortex trajectory for a hovering helicopter.

$$T = b \int_0^{R_T} c \cdot \tfrac{1}{2}\rho\,(\Omega R)^2\, C_\ell\, dR \qquad (14)$$

For an average C_ℓ, this becomes,

$$T = c\, b\, \tfrac{1}{2}\rho\, \Omega^2\, C_\ell\, \frac{R_T^3}{3} \qquad (15)$$

Therefore, combining Eqs. (12) and (15), we have

$$W = \Omega R_T \sqrt{\frac{bC_\ell}{3\pi(R_T/c)}} \qquad (16)$$

For C_ℓ = 0.45 (Ref. 4) and R_T/c = 5.33, which is obtained from our rotor blade geometry, we obtain

$$\frac{W}{\Omega R_T} = 0.134 \qquad (17)$$

For the case given in Fig. 2 (i.e., 3200 rpm with

α=12°), Eq. (17) gives the upward jet velocity W of 29.2 m/s. This value of W in the far wake is consistent with rotor thrust theory since the ratio of the experimentally determined axial velocity of the tip vortex in the near wake to W gives a value of δ = 20.4/29.2 = 0.70.

Equation (17) shows that the upward jet velocity is about 13% of the rotating blade tip velocity, ΩR_T. Therefore, one may neglect the effect of the upward jet velocity W on the calculation of the circumferential vortex velocity. Accordingly, the maximum velocity in the vortex core is approximately given by Eq. (9);

$$v_{max} = \frac{\Omega R_T \, C_\ell \, B}{4\pi (r_o/c)} \quad . \tag{18}$$

However, the complete expression for the maximum velocity in the vortex core v'_{max} is also simple enough to use.

$$v'_{max} = \left\{ v_{max}^2 + (\delta W)^2 \right\}^{\frac{1}{2}} \tag{19}$$

where v_{max} and W are given in Eqs. (18) and (16) respectively.

Of note is that δ the correction factor in W, has the value 0.5 just downstream of the rotor disk and increases to 1 at downstream infinity, which is the so-called half-body theorem.[28] As mentioned earlier, the shadowgraph experiment resulted in the value of δ = 0.70.

The density changes accompanying the flow velocities can be calculated by assuming that the flow outside the core remains isentropic from infinity to r_o. In isentropic flow,

$$\frac{\rho_{min}}{\rho_s} = \left[1 + \frac{\gamma - 1}{2} M_{max}^2 \right]^{-\frac{1}{\gamma - 1}} , \tag{20}$$

where M_{max} is the maximum Mach number based on v_{max} (i.e., v_{max}/a_o). In addition, ρ_{min} and ρ_s are the densities corresponding to v_{max} and stagnation values, respectively.

Of note is that v_{max} depends on (r_o/c) and $\frac{\Omega R_T}{a_o}$ as shown in Eq. (18), as does ρ_{min}/ρ_s.

d. Sensitivity of Shadowgraphs

A shadowgraph is sensitive to the second derivative of the refractive index, n. The change in intensity, I, at a screen located at a distance ℓ is given by Goldstein[29];

$$\frac{\Delta I}{I} = - \frac{\ell}{n_s} \int_o^{r_o} \frac{\partial^2 n}{\partial y^2} \, dr \tag{21}$$

where n is the refractive index, and n_s is that for surrounding air. The integral in Eq. (21) represents the total change due to the passage of light through a characteristic length r_o. In Eq. (21), y represents a coordinate normal to r along which n is changing. The refractive index n depends upon density and is given in Liepmann and Roshko[30] by

$$n = 1 + \beta \, (\rho/\rho_s) \tag{22}$$

where β for air at standard conditions is 0.000292.

Of note is that n_s in Eq. (21) becomes

$$n_s = 1 + \beta \cong 1 \tag{23}$$

Substituting Eq. (22) into Eq. (21), it can be seen that

$$\frac{\Delta I}{I} = - \frac{\beta \ell}{\rho_s} \int_o^{r_o} \frac{\partial^2 \rho}{\partial y^2} \, dr \tag{24}$$

Assuming that

$$\frac{\partial^2 \rho}{\partial y^2} \sim \frac{\Delta \rho}{(\Delta r)^2} \tag{25}$$

we have

$$\frac{\Delta I}{I} \sim - \beta \ell \left(\frac{\Delta \rho}{\rho_s} \right) \frac{r_o}{(\Delta r)^2} \tag{26}$$

Replacing Δρ with $(\rho_{min} - \rho_s)$, and Δr with r_o, respectively, we obtain

$$\frac{\Delta I}{I} \sim \beta \left(1 - \frac{\rho_{min}}{\rho_s} \right) \frac{1}{(r_o/\ell)} \tag{27}$$

If we introduce a visibility function S which is proportional to ΔI/I, we can write S as

$$S = \beta \left(1 - \frac{\rho_{min}}{\rho_s} \right) \frac{1}{(r_o/\ell)} \tag{28}$$

where ρ_{min}/ρ_s is given in Eq. (20), r_o is the vortex core radius corresponding to v_{max}, and ℓ is the distance between the rotor blade and the screen.

e. Calculation of the Visibility Function

The visibility function S varies with the tip Mach number M_T, r_o/c and BC_ℓ for a given c/ℓ.

As mentioned earlier, the correction factor B in v_{max} (i.e., see Eq. (18)) ranged from 0.42 for the turbulent trailing vortex to 0.715 for the laminar one. As an average, the value of 0.5 was used for the correction factor B. The visibility function S was calculated over the range of the tip Mach number M_T and dimensionless vortex core radius r_o/c and is shown in Fig. 8. Other quantities used are given in the following:

$$\begin{aligned} \alpha &= 12° \\ C_\ell &= 0.45 \\ a_o &= 350 \text{ m/s} \\ \ell &= 4.4 \text{ m} \\ R_T &= 0.65 \text{ m} \\ c &= 0.122 \text{ m} \\ \gamma &= 1.4 \end{aligned}$$

Figure 8 demonstrates that the visibility function S decreases with increasing dimensionless core radius, r_0/c. The typical value of r_0/c was experimentally observed to be 0.063, which is indicated by the vertical line noted as "Range of Experiments" in Fig. 8. In addition, the sensitivity function S increases with the tip Mach number M_T.

The threshold value of S for the vortex to be just visible can be determined somewhat approximately by using the results shown in Fig. 9. This is a case for $\alpha = 4°$ and a tip Mach number equal to 0.4 where a vortex was just observed. The core radius ratio was 0.063. Because C_ℓ was not measured directly, there is some uncertainty in its value. Comparing our data to that of Caradona et al[4] who used an airfoil close to this, the average C_ℓ may be estimated to be 0.085. The peak values could be as high as 1.5 times this value. The strength of the tip vortex may relate to either the mean C_ℓ or the maximum. The quantity B which determines the maximum velocity in the vortex ranges from 0.5 to 0.7 as indicated previously. Therefore, the value of BC_ℓ which governs the vortex visibility can take values between 0.0425 to 0.089 as shown in Fig. 9. The spread in the cases of S vs (r_0/c) is substantial. The value of S for a vortex to be just visible is between 0.00013 and 0.0004.

V. Summary and Conclusions

A new experimental shadowgraphy technique using a retro-reflecting screen was developed to observe tip vortices in a full-scale test. Tip vortex trajectories were visible in shadowgraphs for a range of tip Mach numbers from 0.38 to 0.6. The angles of attack ranged from 4° to 14°. Visibility improves with speed and angle of attack. The effect of the angle of attack α was substantial. At an angle of attack greater than 8 degrees, the visibility is significant even at relatively low tip Mach numbers. It can be expected that at higher tip speeds, visibility would be even

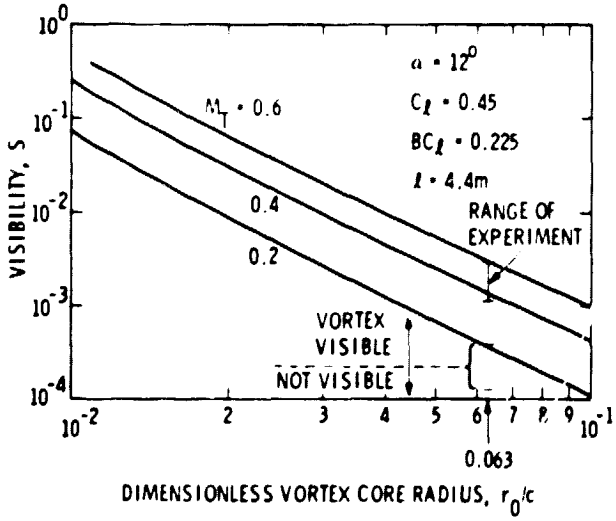

Fig. 8 Visibility as a function of dimensionless core radius for several tip Mach numbers. $C_\ell = 0.45$ $\alpha = 12°$, and $\ell = 4.4$ m.

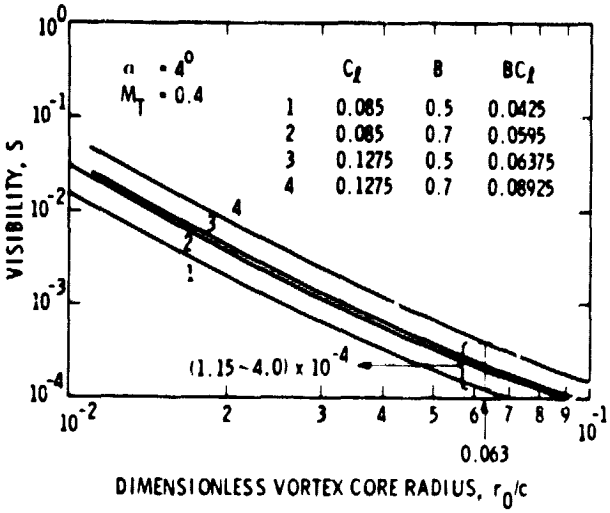

Fig. 9 Visibility vs dimensionless core radius at $M_T = 0.4$ for $\alpha = 4°$ assuming several values of C_ℓ and B.

better. In addition, the size of the vortex core, the axial velocity, and axial and radial vortex core coordinates during the hovering motion could be determined experimentally.

The effect of beam length (i.e., the optical path length between the rotor and the Scotchlite screen) is small; shadowgraphs at $\ell = 4.4$ and 6.4 m look approximately similar. Even greater distances could be used with good results.

A simplified analysis was developed to estimate the influence of angle of attack and tip speed on the visibility of vortices in the shadowgraphs. The circumferential velocity at the vortex core depends on the strength of the tip vortex, and hence on the lift coefficient C_ℓ. The magnitude of velocity in the wake is the resultant of this velocity and the axial jet velocity from the rotor. Assuming isentropic flow outside the tip vortex from the core radius to infinity, the local density change was calculated. The second derivative of the density field integrated along the optical path leads to a measure of visibility of shadowgraphs defined by S. This was calculated as a function of C_ℓ, tip Mach number M_T, vortex core to chord ratio, r_0/c and optical path length. The threshold value of S was found to be approximately 0.00025, above which the vortex core should be visible and below which it may not be.

The present investigation demonstrated that the application of the wide-field shadowgraphy technique to a large wind tunnel or to a full-scale test stand could be made. In addition, the simplicity of this technique should allow use concurrently in other on-going test programs.

ACKNOWLEDGEMENT

Mr. John Kendall from the County of Los Angeles, Sheriff's Department provided the rotor and its clutch box, and Mr. J. Chadwick from the Chadwick-Helmuth Company balanced the rotor with his Vibrex Track and Balance System.

The authors also express appreciation to Messrs. J. Godley, B. Green and R. Smither for their contributions in fabrication and assembly of the test facility and to Dr. Ken Harstad for his assistance in the calculation of the visibility function.

Table 1 Summary of Various Experimental Methods and Test Conditions

Investigator	Method	NACA Airfoil	Aspect Ratio AR	Number of Blades b	Tip Mach Number M_T	Pitch Angle α
Landgrebe[12]	smoke photographs	0012 no twist linear twist	13.5 18.0	2,4,6,8	0.46-0.61	6,8,10, 11
Kocurek and Tangler[15]	Schlieren	0012 no twist twist	7.1 13.5 18.2	1,2,3,4	0.46	0,4,6, 8,10,12
Caradona and Tung[4]	hot-wire anemometer pressure transducers	0012 no twist no taper	6.0	2	0.43-0.79	5,8,12
present investigation	shadowgraphs	0015 twist no taper	5.3	2	0.38-0.64	4,8,12, 14

REFERENCES

1. Landgrebe, A. J. and Cheney, Jr., M. C., "Rotor Wakes-Key to Performance Prediction," AGARD Conf. Proceedings, on "Aerodynamics of Rotary Wings AGARD-CP-111, Marseilles, France, September, 1972.

2. Rabbott Jr., J. P. "Static-thrust measurements of the aerodynamic loading on a helicopter rotor blade." NACATN 3688, Langley Aeronautical Laboratory, National Advisory Committee for Aeronautics, Langley Field, Virginia 1956.

3. Scheiman, J. and Kelley, H. L. "Comparison of flight-measured helicopter rotor-blade chordwise pressure distributions with static two-dimensional airfoil characteristics," NASA TN D-3936 1967.

4. Caradona, F. X. and Tung, C., "Experimental and Analytical Studies of a Model Helicopter Rotor in Hover," Vertica, Vol. 5, pp. 149-161, 1981.

5. Cook, C. V., "The Structures of the Rotor Blade Tip Vortex," AGARD Conf. Proceedings, on "Aerodynamics of Rotary Wings" AGARD-CP-111, Marseilles, France, September, 1972.

6. Landgrebe, A. J. and Johnson, B. V., "Measurement of Model Helicopter Rotor Flow Velocities with a Laser Doppler Velocimeter." J. American Helicopter Soc., Vol. 19, pp. 39-43, 1974.

7. Biggers, J. C. and Orloff, K. L., "Laser Velocimeter Measurements of the Helicopter Rotor-Induced Flow Field," J. American Helicopter Soc., Vol. 20, pp. 2-10, 1975.

8. Desopper, A., "Rotor Wake Measurements for a Rotor in Forward Flight," Internation Conf. Rotorcraft Basic Research, Research Triangle, N.C., Feb. 1985.

9. Yu, Y. H. and Kittleson, J. K., "Reconstruction of a Three-Dimensional, Transonic Rotor Flow Field from Holographic Interferogram Data," International Conf. Rotorcraft Basic Research, Research Triangle, N.C., Feb. 1985.

10. Jenney, D. S., Olson, J. R. and Landgrebe, A. J., "A Reassessment of Rotor Hovering Performance Prediction Methods," J. American Helicopter Soc., Vol.13, pp. 1-26, 1968.

11. Lynn, R. R., Robinson, F. D., Batra, N. N. and Duhon, J. M., "Tail Rotor Design, Part 1: Aerodynamics," J. American Helicopter Soc., Vol. 15. pp. 2-15, 1970.

12. Landgrebe, A. J., "The Wake Geometry of a Hovering Helicopter Rotor and Its Influence on Rotor Performance," J. American Helicopter Soc., Vol. 17, pp. 3-15, 1972.

13. Tangler, J. L., "Investigation of the Stability of the Tip Vortex Generated by

Hovering Propellers and Rotors," Atmospheric Flight Mechanics Conf., 2nd, Palo Alto and Moffett Field, CA, September, 1972.

14. Sonnerborn, W.G.O. and Drees, J. M., " The Scissors Rotor," J. American Helicopter Soc., Vol. 20, pp. 18-27, 1975.

15. Kocurek, J. D. and Tangler, J. L., " A Prescribed Wake Lifting Surface Hover Performance Analysis," J. American Helicopter Soc., Vol. 22, pp. 24-35, 1977.

16. Clark, D. R. and Leiper, A. C., "The Free Wake Analysis; A Method for the Prediction of Helicopter Rotor Hovering Performance," J. American Helicopter Soc., Vol. 15, pp. 3-11, 1970.

17. Landgrebe, A. J., "An Analytical and Experimental Investigation of Helicopter Rotor Hover Performance and Wake Geometry Characteristics," USAAMRDL Technical Report 71-24, June 1971.

18. Parthasarathy, S. P., Cho, Y. I. and Back, L. H., "Fundamental Study of Flow Field Generated by Rotorcraft Blades using Wide-Field Shadowgraph," JPL Publication D-2064, Dec. 1984.

19. McCormick, B. W., Tangler, J. L., and Sherrieb, H. E., "Structure of Trailing Vortices," J. Aircraft, Vol. 5, No. 3, pp. 260-267, 1968.

20. Bate, Jr., E. R., "Aircraft Wake Modeling: Preliminary Design Aspects," Aerovironment Inc., AV FR 445, Aug. 1974.

21. Squire, H. B., "The Growth of a Vortex in Turbulent Flow," Aeronautical Quarterly, Vol. 16, pp. 302-306, 1965.

22. Mason, W. H., and Marchman III, J. F., "Far-Field Structure of Aircraft Wake Turbulence," J. Aircraft, Vol. 10, No. 2, pp. 86-92, 1973.

23. Corsiglia, V. R., Schwind, R. G., and Chigier, N. A., "Rapid Scanning, Three-dimensional Hot-wire Anemometer Surveys of Wing Tip Vortices," J. Aircraft, Vol. 10, No. 12, pp. 752-757, 1973.

24. Lamb, H., Hydrodynamics, Dover 1932, p. 592.

25. Govindaraju, S. P., and Saffman, P. G., "Flow in a Turbulent Vortex," Physics of Fluids, Vol. 14, No. 10, pp. 2074-2080, 1971.

26. Hoffman, E. R., and Joubert, P. N., "Turbulent Line Vortices", J. Fluid Mechanics, Vol. 16, pp. 395-411, 1963.

27. Dwinnell, J. H., Principles of Aerodynamics, McGraw-Hill, 1949, pp. 210-214.

28. Prandtl, L., Essentials of Fluid Dynamics, Blackie & Son Ltd. 1960, pp. 203-226.

29. "Measurements in Heat Transfer," Edited by Eckert, E. R. G., and Goldstein, R. J., McGraw-Hill, N.Y., 1976, p. 257, Chpt. 5, Goldstein, R. J., "Optical Measurement of Temperature."

30. Liepmann, H. W., and Roshko, A., "Elements of Gasdynamics," John Wiley & Sons, Inc., 1957, p. 154.